Title: Maternal hyperglycemia impedes second heart field-derived cardiomyocyte differentiation to elevate the risk of congenital heart defects

Authors: Sathiyanarayanan Manivannan[1,2#], Corrin Mansfield[1,2#], Xinmin Zhang[3], Karthik. M. Kodigepalli[4], Uddalak Majumdar[1,2], Vidu Garg[1,2,5,6*] and Madhumita Basu[1,2,5*]

Affiliations:

[1] Center for Cardiovascular Research, Abigail Wexner Research Institute at Nationwide Children's Hospital, Columbus, Ohio, United States of America. [2] Heart Center, Nationwide Children's Hospital, Columbus, Ohio, United States of America. [3] BioInfoRx Inc. Madison, Wisconsin. [4] Department of Pediatrics, Medical College of Wisconsin, Milwaukee, Wisconsin, United States of America. [5] Department of Pediatrics, The Ohio State University College of Medicine, Columbus, Ohio, United States of America.[6] Department of Molecular Genetics, The Ohio State University, Columbus, Ohio, United States of America.

# Indicates equal contribution

* Co-corresponding authors

✉**lead contact:**

Madhumita Basu, Ph.D. Center for Cardiovascular Research and The Heart Center, Nationwide Children's Hospital, Room WB4235, Columbus, OH 43205. Phone: 614-355-5826, Fax: 614-355-5725, Email: Madhumita.Basu@nationwidechildrens.org

Total word count: 14,393

Abstract:

Congenital heart disease (CHD) is the most frequently occurring structural malformations of the heart affecting ~1% of live births. Besides genetic predisposition, embryonic exposure to teratogens during pregnancy increases the risk of CHD. However, the dose and cell-type-specific responses to an adverse maternal environment remain poorly defined. Here, we report a dose-response relationship between maternal glucose levels and phenotypic severity of CHD in offspring, using a chemically-induced pregestational diabetes mellitus (PGDM) mouse model. Embryos from dams with low-level maternal hyperglycemia (matHG) displayed trabeculation defects, ventricular wall thinning, and ventricular septal defects (VSD). On the other hand, embryos from dams with high-level matHG display outflow tract malformations, ventricular wall thinning and an increased rate of VSD. Our findings show that increasing levels of matHG exacerbates CHD occurrence and severity in offspring compared to control embryos. We applied single-cell RNA-sequencing to define matHG-related transcriptional differences in E9.5 and E11.5 hearts as comparing to controls. Disease-dependent gene-expression changes were observed in *Isl1*$^{+}$ second heart field (SHF) and *Tnnt2*$^{+}$ cardiomyocyte subpopulations. Lineage tracing studies in *Isl1-Cre*; *Rosa*^{mTmG} embryonic hearts showed *Isl1*$^{+}$-SHF-derived cardiomyocyte differentiation was impaired with matHG. This study highlights the influence of matHG-dosage on cardiac morphogenesis and identifies perturbations in the *Isl1*-dependent gene-regulatory network that affect SHF-derived cardiomyocyte differentiation contributing to matPGDM-induced CHD.

One Sentence Summary:

Profiling of single-cell transcriptomics and SHF cell-fate identifies intrinsic deficits in cardiomyocytes that contribute to maternal diabetes-associated CHD.

Introduction:

Congenital heart disease (CHD) is defined as gross structural malformations of the heart and/or great vessels and is the most common form of all birth defects. It affects nearly 40,000 live births per year in the United States and contributes to a significant fraction of childhood mortality (*1, 2*). CHD is proposed to have a multifactorial etiology, and its phenotypic manifestation is likely the result of a combination of genetic and environmental contributors (*3*). The genetic basis of CHD has undergone significant investigation, and a disease-causing genetic abnormality is identified in ~20-30% of all cases (*4-7*). Yet, these genetic lesions often fail to explain phenotypic variability among CHD patients with identical genetic variants. In many cases, the phenotypic differences are ascribed to intrauterine environmental disturbances (*8, 9*). These environmental causes of CHD include maternal illnesses, viral infections, and therapeutic and nontherapeutic drug exposures (*10, 11*). Among these maternal environmental contributors to CHD, a strong correlation has been identified between maternal pre-gestational diabetes mellitus (matPGDM) and the increased occurrence of CHD. Estimates from the Center for Disease Control (CDC) reflect that ~8% of CHD is a result of uncontrolled maternal diabetes that is present before and during the first trimester of pregnancy (*12, 13*). It is therefore important to elucidate the role of the fetal environment which "compromises at-risk genotype" to increase the incidence of disease and contribute to phenotypic variability in CHD patients harboring identical genetic variants.

Clinical and epidemiological studies have identified several subtypes of CHD in infants of diabetic mothers (*14*). These CHD phenotypes range from laterality defects, transposition of great arteries, outflow tract (OFT) defects with normally-related great arteries, double outlet right ventricle (DORV), cardiac septal defects (ASD, VSD, AVSD) to hypoplastic left heart syndrome (*13-15*). In a nationwide cohort study, the authors emphasized that the infants of diabetic mothers have a greater risk of conotruncal heart defects, which are a subgroup of CHD that includes malformations of the cardiac OFT and great arteries. This CHD subtype involves cardiac structures that are derived from the cardiac neural crest and the secondary heart field cell lineages (*16*). In addition, studies in rodent models of matPGDM recapitulate these CHD phenotypes and reaffirm the significance of gene-environment interaction contributing to diabetic embryopathy (*17, 18*). Yet, how varying levels of maternal blood glucose lead to structural defects and alter cell-type-specific transcriptional programs in the early embryonic heart during pregnancy remains undefined.

A meta-analysis of maternal diabetes-exposed offspring was consistent with experimental study findings which suggests a role for maternal hyperglycemia (matHG) affecting cardiac structures originating from anterior or second heart field (SHF)(*13, 14*). However, the glucose-sensitivity of this progenitor cell population has not been tested. During the early stages of cardiac development, the anterior and posterior SHF (aSHF/pSHF) contribute cardiac progenitor cells to the arterial and venous poles of the heart, which occurs at E8.0 and E10.5 of mouse gestation (comparable to 3-5 weeks of human gestation), and drive the linear heart tube extension during looping

morphogenesis (*19*). Retrospective cell-lineage analysis studies in avian models and mouse embryos demonstrated that SHF gives rise to the OFT, right ventricle (RV), and atrial myocardium (*20, 21*). In terms of cell types, SHF progenitor cells differentiate into the cardiomyocytes, smooth muscle cells, and endocardial/endothelial cells. This specification of multipotent SHF cells and subsequent differentiation processes are mediated by a coordinated series of chromatin rearrangements and transcriptional regulation (*19, 22*). Perturbations in transcription factors (TFs) (Isl1, Nkx2.5, Gata4), gene-regulatory proteins (Tbx1, Mef2c, Hand2), intercellular signaling pathways (Bmp, Shh, Wnt, Notch), and chromatin remodeling factors (Smarca4, Smarcd3, Smarcc1) affect SHF deployment and when disrupted or deleted in mice have been demonstrated to cause a high rate of conotruncal and septal defects (*21, 23, 24*). These genes stabilize the SHF specification, differentiation, and proliferation and regulate their derivatives to ensure normal development (*19, 23*). We and others have independently demonstrated that embryonic exposure to matHG is a disruptor of gene-expression of core cardiac TFs and epigenetic modifiers, and disrupts signaling pathways involving Notch, Wnt, Bmp, Tgfβ, Vegf, Shh, Hif1α-pathways in the developing heart (*17, 25*). The gene-environment interaction studies in mice between matPGDM and *Notch1*, *Nkx2.5*, *Ask1*, *Hif1α* haploinsufficiency demonstrated an increased incidence of VSD, DORV and truncus arteriosus in diabetic offspring compared to controls (*17, 26-29*). While these studies highlight the need to understand the effect of matPGDM in cardiac development, the effect of hyperglycemic dosage on (i) cardiac development and disease severity and

(ii) transcriptional changes in multiple cell lineages is lacking which impedes our knowledge in understanding the developmental toxicity elicited by matHG.

Here, we used the streptozotocin (STZ)-induced murine model of matPGDM to determine the influence of hyperglycemic levels on cellular and molecular derangements in embryonic hearts. The spectrum of cardiac defects in wildtype hearts exposed to low and high levels of matHG at E9.5, E11.5, E13.5 and E15.5 developmental stages were characterized and compared against control (CNTRL) embryos. The embryos subjected to matHG exhibited a dose-dependent increase in septal defects, OFT and AVC cushion anomalies and ventricular chamber malformations, suggesting cellular perturbations and transcriptional misregulation in cardiac progenitors and their derivatives. To provide direct evidence of altered gene-expression upon hyperglycemic exposure *in utero*, we performed 10xGenomics single-cell RNA-sequencing (scRNA-seq) in CNTRL and matHG-exposed E9.5 and E11.5 hearts. Bioinformatic analyses identify HG-mediated key differences in gene-expression in SHF cells, marked by *Isl1*, and in *Tnnt2*$^{+}$ cardiomyocytes. Gene expression analysis revealed significant changes in SHF and BMP populations in E9.5 embryos, and in the atrial and ventricular CMs and OFT in E11.5 embryos when exposed to matHG. Furthermore, comparative cell-fate mapping studies between CNTRL and matHG-exposed *Isl1-Cre*$^{+}$*; Rosa*$^{mT/mG}$ embryonic hearts identify SHF-derived myocardial differentiation defects in embryos subjected to matHG. Together, this study uncovers the dose-response impact of matHG on multiple aspects of cardiac development and scRNA-seq data prioritizes the cellular subtypes that are major contributors to matPGDM-induced CHD.

Results:

Maternal PGDM-induced cardiac malformations are dosage-sensitive

To determine if the level of matHG affected the phenotypic spectrum of CHD observed in the diabetic offspring, we treated wildtype (*wt*) female mice with streptozotocin (STZ), and generated diabetic mice that mimicked human type 1 diabetes mellitus (*26, 30*). STZ-treated hyperglycemic and non-STZ-treated wildtype C57BL/6J (*wt*) females were then bred to adult *wt* males. Embryos were collected at E9.5, E11.5, E13.5 to examine the effect of matHG dosage on different aspects of embryogenesis with particular attention to cardiac development (**Fig. 1A**). Maternal blood glucose (B.G.) levels in the *wt* females were measured 7-14 days post-STZ injection to confirm the hyperglycemic status and at the time of embryo harvest following our previously published protocol (*26*). Here, we noticed a similar dose of STZ treatment in the experimental group resulted in a wide range of hyperglycemia during embryo harvest likely due to variability in β-cell toxicity. The maternal B.G. levels of STZ-treated females during embryo harvest ranged from 209-639 mg/dl and were found to be significantly greater than non-STZ treated CNTRL mice (**Fig. 1B**). Using the terminal B.G. levels, we divided our experimental embryos at E9.5, E11.5 and E13.5 embryos into low-matHG (270.9±32.8 mg/dl) and high-matHG (447.1±120.3 mg/dl) exposure groups. They were compared against CNTRL embryos with average maternal B.G. (187.6±21.1 mg/dl) to evaluate the effect of mild and severe matHG on embryonic development with a focus on cardiac morphogenesis (**Fig. 1C**). There were no significant changes in average litter size at

different developmental time points in each of these three conditions (**Table S1**). Upon gross morphological analysis, we noticed that embryos subjected to high-matHG demonstrated reduced body size, pericardial effusion, hemorrhaging and neural tube defects when compared to low-matHG and CNTRL groups (**Fig. S1A-C**). The E9.5, E11.5 and E13.5 hearts exposed to low and high-matHG were then examined for cardiac abnormalities. Histologic analysis of low vs. high-matHG-exposed embryos revealed a statistically significant increase in the rate of CHD compared to CNTRL embryos at each of these time points (**Table 1**). At E9.5, a spectrum of myocardial anomalies was noted and included myocardial thinning, trabeculation defects, increased endocardium-myocardial (EC-CM) distance (Fig. 2A-D). There was an increased incidence of cardiac abnormalities with low (3/20=15%) and high levels (6/24=25%) of matHG compared to no malformations noted in CNTRL embryos (0/23 = 0%; p = 0.041). At E11.5, hypocellular OFT and atrioventricular canal (AVC) cushions were seen at both low and high-levels of matHG (**Fig. 2E-H**). The incidence increased in low-matHG (5/23 = 21.7%) and high matHG exposure (7/23=30.4%) which was significantly greater than CNTRL (0/25 = 0%; p = 0.014) embryos (**Table 1, Fig. 1D-L and Fig. 2A-H**). Dose-dependent increased rate of myocardial (RV and LV wall) thinning and VSD was found in low (4/20 = 20%) and high (9/25 = 36%) matHG-exposed E13.5 embryos when compared to CNTRL embryos (0/26 = 0%; p = 0.004) (**Table 1, Fig. 1M-R and Fig. 2I-L**). More complex cardiac defects were noticed in E13.5 embryos exposed to high-matHG which resulted in truncus arteriosus, VSDs with an overriding aorta, thin RV and LV myocardial wall with disorganized trabeculae, and single ventricle-like phenotype, as we previously reported (**Fig. 1Q, R**)

(*26*). We also extended our analysis to evaluate the influence of matHG exposure at E15.5, when the majority of cardiac morphogenetic events have been completed (**Fig. S1D**). At this timepoint, the differences in maternal B.G. levels between low (301.0 $\pm$ 9.9mg/dl) and high-matHG (555.7 $\pm$ 152.9 mg/dl) groups were statistically significant when compared to CNTRL (193.7 $\pm$ 11.4 mg/dl) mice (**Fig. S1E**). Gross morphological defects were observed in high-matHG exposed embryos compared to low-matHG and CNTRL embryos (**Fig. S1F-J**). Compared to normal development in CNTRL E15.5 embryos (0/21 = 0%), histological analysis revealed cardiac defects including VSD, ventricular hypertrabeculation, thickened semilunar valves in both low (2/26 =7.7%) and high (4/24 =16.7%) matHG-exposed embryos (**Fig. S1K-P**). We also noticed the presence of PTA and myocardial thinning in E15.5 hearts when exposed to high-matHG levels (**Fig. S1O**). Collectively, we demonstrated matHG exposure causes a spectrum of CHD including septal and myocardial defects along with impaired OFT and AVC cushion formation. Our phenotypic characterization of matHG-exposed embryos established the dose-dependent influence of matHG on critical stages of heart development.

Single-cell transcriptomics reveals diverse cellular response to matHG exposure

To capture the underlying cellular basis of matHG-driven cardiac defects, we performed scRNA-seq in CNTRL and matHG-exposed developing hearts. We micro-dissected E9.5 and E11.5 whole hearts from the embryos of CNTRL *wt* dams (maternal B.G. of 145mg/dl at E9.5 and 196mg/dl at E11.5) and hyperglycemic dams (maternal B.G. of 312mg/dl at E9.5 and 316mg/dl at E11.5). Embryos from each litter were pooled,

dissociated and processed to obtain single-cell libraries using the 10xGenomics Chromium controller and 3' polyA-based gene expression analysis kit. The libraries were sequenced together to avoid batch effects (**Fig. 3A**). We obtained 11,987 single-cell transcriptomes from both CNTRL and matHG-exposed E9.5 and E11.5 embryonic hearts. Using Seurat-based unsupervised clustering, we identified 14 clusters of cells (0-13) based on the top five maker gene expression per cluster (**Fig. S2A-D**). Cells marked with non-mesodermal markers were found in clusters 3, 6, 7, 11 and 12 and were removed from further analysis (**Fig. S2C, E-G**). Finally, a total of 8503 single-cell transcriptomes were re-clustered into six broadly defined cardiac populations and were used to compare cell-type-specific differences in gene expression between CNTRL and matHG-exposed E9.5 and E11.5 hearts (**Fig. 3B-D**). We assigned cardiac identities to six distinct clusters based on the expression of key marker genes detected in respective clusters (**Fig. 3C)**. These clusters represent *Isl1*$^{+}$ multipotent progenitor (MP), *Tnnt2*$^{+}$ cardiomyocytes (CM), *Dlx5*$^{+}$ neural crest (NC), *Chd5*$^{+}$ endocardial/endothelial (EC), *Postn*$^{+}$ fibromesenchymal (FM) and *Wt1*$^{+}$ epicardial (EP) cells. The cluster-specific expression of markers was validated using our data (**Fig. S3A**) and other published scRNA-seq datasets in *wt* embryonic hearts (*31, 32*). We next examined the cell-type-specific effect of matHG in CNTRL vs. matHG-exposed hearts at E9.5 and E11.5 (**Fig. 3E**). At E9.5, marked changes in cellular distribution was noted in MP (19.3% in CNTRL vs. 17.0% in matHG), NC (9.8% in CNTRL vs. 26.4% in matHG), EP (13.4% in CNTRL vs. 3.9% in matHG) and FM (5.4% in CNTRL vs. 1.5% in matHG) cells (**Fig. 3E**). This data suggests that matHG affects the allocation of myocardial precursors, neural crest cells, and endocardial/endothelial-to-

mesenchymal (EndoMT)-derived cells, the cell types known as mediators of conotruncal malformations. In comparison, subtle changes were observed in CM (38.2% vs. 38.9%), EC (13.8% vs. 12.3%) between CNTRL and matHG-exposed embryos at E9.5. However, at E11.5, matHG-exposed hearts displayed noticeable changes in MP (11.6% in CNTRL vs. 7.9% in matHG), CM (30.9% in CNTRL vs. 47.1% in matHG) and FM (17.6% in CNTRL vs. 5.9% in matHG) cells. Modest changes in NC (3.5% in CNTRL vs. 1.5% in matHG), EP (14.4% in CNTRL vs. 11.0% in matHG) and EC (21.9% in CNTRL vs. 26.4% in matHG) cells were also observed with HG exposure at E11.5 (**Fig. 3D, E**). The temporal differences in cellular distribution between CNTRL vs. matHG-exposed support previous publications showing defects in HG-mediated EndoMT and neural crest cell migration in the murine model of matPGDM (*30, 33*). In summary, using a combination of detailed phenotyping and *in vivo* scRNA-seq, we describe the direct influence of matHG on cell-type specific responses during the early cardiac developmental stages.

Hyperglycemia triggers gene-expression changes in cardiac progenitor cells and cardiomyocytes

The occurrence of myocardial, OFT, and septal defects in the E9.5, E11.5 and E13.5 hearts exposed to matHG (shown in **Fig. 1 and 2**) suggested that cardiac progenitor cells and their derivatives (cardiomyocytes) are affected by maternal hyperglycemic state. We, therefore, focused on the transcriptional profiles of MP and CM clusters at CNTRL and HG-exposed E9.5 and E11.5 hearts and performed differential gene expression analysis implemented in Seurat.

First, using a stringent cutoff value ($log_2FC \leq -1$ or $\geq +1$ and $P_{adj} \leq 0.05$), we found 262 differentially expressed genes (DEGs) in *Isl1*$^+$ MP cluster at E9.5 (**Table S2**). Gene Ontology (GO) analysis with DEGs in this cluster showed perturbations in biological processes associated with (i) regionalization, anterior-posterior pattern specification, cell fate commitment, (ii) cardiomyocyte, mesenchymal and neural crest cell differentiation, and (iii) cardiac ventricle and septum development (**Fig. S3B, Table S4**). The genes associated with these processes include Hox-family members, fibroblast growth factors, Forkhead box members, T-box TFs, muscle-specific TFs and regulators of SHF development (**Table S2**). HG-mediated differential expression of these genes indicates that disruption of cardiac progenitor cell commitment could alter cardiomyocyte fate.

Second, the expression analysis in *Tnnt2*$^+$ CMs between CNTRL and matHG-exposed hearts at E9.5 and E11.5 displayed 357 and 326 DEGs, respectively (**Table S2 and S3**). GO analysis of DEGs in E9.5 and E11.5 CMs revealed biological processes linked to (i) muscle contraction and myofibril assembly, (ii) regulation of ion transport, (iii) cardiac muscle cell differentiation and proliferation, (iv) regulation of Wnt, Bmp, TGF and MAPK signaling pathways, (v) response to hypoxia, (vi) H3K4 trimethylation, (vii) mitochondrial organization with regulation of the metabolic processes such as tricarboxylic acid cycle in the setting of maternal HG environment (**Fig. S3C, D, Table S4, S5**). In E9.5 CMs, we found most DEGs are associated with the differentiation markers, voltage-gated calcium-channels and potassium channels, regulators of cardiac contractility, transcriptional and chromatin regulators. Whereas the determinants of sarcomere assembly and cardiac muscle function, myocardial TFs, Bmp, TGF and EGF

receptor family genes, glucose and mitochondrial metabolism genes were significantly perturbed in E11.5 CM with matHG. Many studies in human subjects and rodents provide evidence that impairments in the key components of CM function and metabolism lead to a spectrum of CHD and heart failure in adults with metabolic syndrome (*34*). Thus, single-cell gene expression analysis shows direct evidence of the developmental toxicity of matHG and found transcriptional differences in key TFs and signaling pathways in cardiac progenitor cells and cardiomyocytes. This data also suggests that deregulated expression in cardiomyogenic cell lineages is likely contributing to SHF-derived structural defects seen in matHG-exposed embryonic hearts.

Cardiac progenitors and cardiomyocyte subpopulations show diverse response to matHG

To determine the effect of matHG on multipotent progenitor and cardiomyocyte subpopulations, we performed a sub-clustering analysis on the integrated E9.5 and E11.5 scRNA-seq data (**Fig. 4A**). We identified two subpopulations, anterior/posterior SHF and branchiomeric muscle (BMP) progenitors in the MP cluster. While CM reclustering revealed four subpopulations, outflow tract (OFT), atrioventricular canal (AVC), and atrial (Atr) and ventricular myocytes (Ven), based on the expression of top five markers assigned to each cluster (**Fig. 4B**). Markers for each of these sub-cell types are shown in **Fig. S4A-D**, and are consistent with previous reports (*31, 32*). We evaluated the change in the number of cells in each of these sub-clusters at different timepoints and with matHG (**Fig. 4C, D**). We found a higher proportion of BMP cells (2.8% in CNTRL vs. 10.8% in

matHG) at E9.5 but significant decrease in SHF populations both at E9.5 (30.7% in CNTRL vs. 19.6% in matHG) and E11.5 (26.1% in CNTRL vs. 14.1% in matHG). Given the contribution of progenitor cells to the embryonic heart, the reduced number of progenitor cells forebodes the development of a spectrum of CHD in diabetic offspring. This is further reflected in the reduction of *Tnnt2*$^{+}$ OFT-CM (18.7% in CNTRL vs. 3.7% in matHG) and AVC-CM (3.3% in CNTRL vs. 0.6% in matHG) at E11.5, indicating that a reduction in cell numbers could lead to abnormal OFT and AVC development observed in E11.5 and E13.5 embryos (**Fig. 1J, L and Fig. 2F, G**). In contrast, we noticed CNTRL vs. matHG-exposed Atr- (17.0% vs. 14.4%) and Ven-CMs (33.0% vs. 27.6%) were modestly reduced at E9.5, but their proportion was increased by E11.5 (from 16.6% to 26.0% Atr-CM and from 34.2% to 55.1% Ven-CM, respectively), in matHG environment (**Fig. 4C, D**).

To characterize the transcriptional changes in the CM subpopulations, we examined a stage-specific gene regulatory network (GRN) comprising cardiac TFs and known SHF-regulators (Nkx2-5, Mef2c, Gata4 and Tbx5), those are frequently associated with OFT and septal defects in humans and mice (*35-37*). In our scRNA-seq data, we found that *Nkx2-5* expression was markedly diminished in OFT-CM, *Tbx5* expression was downregulated in both Atr- and Ven-CM, whereas *Mef2c* and *Gata4* expression was downregulated in all CM-subpopulations at matHG-exposed E11.5 embryos (**Fig. S4E**). This was followed by a significant reduction in cardiomyocyte maturation genes, including *Ttn*, *Ppargc1a*, *Ctnnb1,* and *Atp2a2* in matHG-exposed AVC, OFT, Atr and Ven-CMs at

E11.5 (**Fig. S4E**). In summary, this data suggests that elevated glucose could induce defective cardiomyocyte maturation by altering the expression of key cardiac genes.

GO analysis was performed on MP-CM DEGs and significantly enriched biological processes ($P_{adj} \leq 0.05$) were compared between two developmental timepoints (**Fig. 4E, Table S6-S8**). The DEGs in E9.5 SHF-derived cells were enriched in processes related to cell proliferation/differentiation; anterior-posterior pattern specification, as described earlier. DEGs in Ven-CM displayed changes in chamber development, muscle cell membrane polarization, muscle contraction. In contrast, OFT, Atr and Ven-CM at E11.5 hearts showed differences in gene expression related to response to stress, muscle cell differentiation, muscle contraction, ATP-dependent metabolic processes, chromatin modification and cell cycle (**Fig. 4E, Table S6-S8**). Therefore, DEG analysis on MP-CM subpopulations shows the spatiotemporal response to matHG during critical stages of heart development.

To test the temporal impact of matHG on the transcriptional differences observed in MP-CM cell lineages, we performed pseudotime ordering of CNTRL and matHG-exposed E9.5 and E11.5 cells using both Monocle (version 2.0) and Slingshot (version 1.8.0). The pseudotime analysis revealed five distinct cell states (state 1-5), where the trajectory started with distinct SHF (state 1) and BMP (state 5) progenitor cells and split into three CM-fates. State 2 was predominantly comprised of OFT-CM with differentiated OFT-CM positioned at state 4. While states 3 and 4 were found to be primarily occupied with AVC, Atr- and Ven-CM populations (**Fig. S5A-D**). Significant differences in the cell numbers/states were found at the two developmental time points with each maternal

condition (**Fig. 4F, Fig. S5B**): (i) at E9.5, a reduction in SHF cell number (state 1) and increase in the proportion of BMP cells (state 5) was noted in matHG-exposed embryos. BMP cells were also found to contribute more to OFT-CM (state 2) under matHG than that is observed under CNTRL; (ii) at E9.5, cells expressing Atr- and Ven-CM markers were found to form a distinct cluster in the trajectory (state 2) which was not seen in CNTRL-exposed embryos; (iii) at E11.5, there was a significant reduction in SHF-derived OFT-CMs in both state 2 and state 4 in matHG embryos; (iv) differentiated CMs (state 4) were present in both CNTRL and matHG exposed embryonic hearts. In contrast, cells in state 3 that correspond to undifferentiated cells of the Atr- and Ven-CMs subpopulation were increased with matHG (**Fig. 4F**). In conclusion, gene expression analysis at the single-cell level suggests that myocardial subpopulations show diverse responses to matHG-exposure during cardiogenesis. Likewise, the pseudotime trajectory predicted that by E11.5, the transcriptional profile of embryonic OFT and chamber myocardium are significantly impacted when subjected to a matHG environment.

Transcriptional analysis of pseudotime states reveals CM differentiation defects with matHG exposure

To identify the markers associated with SHF-derived myocardial impairment under matHG, we performed DEG analysis of the five pseudotime states. The cellular identities were superimposed with progenitor (states 1 and 5) and myocardial lineages (states 2-4) as described earlier (**Fig 4F** and **Fig. 5A**). In each of the pseudotime states, we identified DEGs in CNTRL and matHG-exposed embryos (**Fig. S5E, Table S9, S10**).

The maximum number of DEGs at E9.5 were found in *Isl1*$^{+}$ SHF at state 1 and in less differentiated *Tnnt2*$^{+}$CM subpopulations at state 3. These perturbations in SHF gene regulation and CM subpopulations suggest severe myocardial defects underlie the cardiac defects found in high-matHG exposed E11.5 and E13.5 hearts by histologic analysis. In contrast, the E11.5 pseudotime trajectory displayed prominent deficits in OFT-CM at state 2 and variabilities in Ven- and Atr-CMs between states 3 and 4 (**Fig. 5B**). DEG analysis at E11.5 OFT-CM showed concomitant downregulation of *Itm2a, Cxcl12*, *Hand1, Hand2, Tgfβ2* (**Fig. 5C**), these genes play a critical role in OFT morphogenesis and are implicated in conotruncal CHD (*32, 37-39*). Genes associated with Ven-CM maturation and sarcomeric assembly, *Igf2r* and *Ttn* were significantly downregulated in state 3, but transcriptional coactivator of the p300/CBP-mediated transcription complex, *Cited1* expression was upregulated in state 3 (**Fig. 5D**). Expression of *Cited1* is also increased in matDM-exposed kidneys and is accompanied with decreased expression of the intracellular domain of Notch1 and canonical Wnt targets (*40*), suggesting common pathways triggered in matHG. *Ryr2* expression in matHG-exposed Atr-CM was found to be significantly downregulated, while *Actn2* and *Ankrd1* were upregulated in state 3. In cardiomyocytes isolated from STZ-induced diabetic rats, Ryr2 protein levels were shown to be depleted due to hyperphosphorylation that significantly altered Ca^{2+} transients (*41*). Conversely, genetic variations and altered expression of human *ANKRD1*, *ACTN2* and *TTN* genes are associated with hypertrophic and dilated cardiomyopathies (*42, 43*). In state 4, matHG-exposed CM is characterized by low *Ttn*$^{+}$ expressing cells and displays changes in metabolic genes compared to

CNTRL-CM (**Table S9, S10**). Together, the scRNAseq data suggest that *Isl1*$^{+}$ SHF at E9.5 is reactive to the matHG environment and impairs CM differentiation by perturbing the expression of key metabolic and differentiation genes in their precursors.

SHF-fate mapping analysis under matHG milieu displays cardiomyocytes differentiation defects

To understand the fate of cardiomyocytes derived from *Isl1*$^{+}$ SHF cells upon matHG exposure, we first examined the changes in the expression of *Isl1* and *Tnnt2 from* E9.5 to E11.5 along the pseudotime trajectory (**Fig. 6A**). We found significant downregulation of *Isl1* in matHG-exposed E9.5 SHF and OFT-CM at E11.5, suggesting that these SHF-derived cardiomyocytes are have differentiation defects (**Fig. 6A**). Likewise, *Tnnt2* expression in E9.5 AVC and OFT was significantly downregulated with matHG while differences between Atr- and Ven-CM became more appreciable at E11.5 between states 3 and 4 (**Fig.S4A, B** and **Fig. 6A**). To confirm the scRNA-seq data and to examine if SHF-derived CM differentiation is affected *in vivo*, we used the Isl1-Cre lineage tracing mouse model. Hyperglycemic and CNTRL *Rosa*$^{mT/mG}$ females were bred with *Isl1-Cre*$^{+}$ males and E9.5, E11.5, and E13.5 embryos were harvested for molecular analysis (**Fig. 6B**). The combined average maternal B.G. levels between CNTRL (214.3 $\pm$ 27.6 mg/dl) and matHG-exposed (471.3 $\pm$ 182.9 mg/dl) groups was statistically significant as shown in **Fig. 6C** and **Table S11**. The expression of GFP in *Isl1-Cre*$^{+}$*;* *Rosa*$^{mTmG/+}$ embryos recapitulates the endogenous *Isl1* expression in pharyngeal mesoderm, cardiac OFT, and foregut endoderm at E9.5 (**Fig. S6A**) (*44*). The expression

was extended to regions of midbrain, forebrain, all cranial ganglia, spinal motor neurons, dorsal root ganglia, sinus venosus, and in the posterior hindlimb at *Cre*$^{+}$ E11.5 and E13.5 embryos (**Fig. S6A**), as also shown by other investigators (*44*). Then, we performed co-immunostaining on the tissue sections with α-GFP (marking Isl1-derived cells) and α-Tnnt2 to map SHF-derived CMs as the embryos developed in CNTRL and HG maternal environments. This immunostaining-mediated cell-fate mapping revealed an overall reduction in the number of GFP^{+}Tnnt2^{+} cells in matHG-exposed E9.5 hearts compared to CNTRL *Cre*$^{+}$ embryos. This supports the scRNAseq data that *Isl1*-derived CMs undergo impaired differentiation upon matHG stress (**Fig. 6D-G, P**). Isl1^{+} SHF cells contribute to both CMs and ECs (*45*). Therefore, we also checked the impact of matHG on SHF-derived EC cells using the scRNAseq data (**Fig. S6B, C)** and through histological examination of the embryos (**Fig. S6D)**. No obvious differences were found in GFP^{+}Emcn^{+} cells marking SHF-derived ECs in matHG-exposed *Is1l-Cre*$^{+}$*; Rosa*$^{mTmG/+}$ embryos (**Fig. S6D**). The *Isl1*-driven expression of GFP reporter was further traced at later time points (E11.5 and E13.5) and compared between CNTRL and matHG-exposed *Cre*$^{+}$ embryos. The Isl1-derived CMs at matHG exposed E11.5 hearts were found to be consistently downregulated in OFT and atria with a trend of downregulation in the RV (**Fig. 6H-K, P**). At E13.5, however, we demonstrated significant downregulation of GFP^{+}Tnnt2^{+} cells in both the OFT and RV (**Fig. 6L-P**).

The number of cardiomyocytes in the developing heart is determined by both the proliferation of the precursor multipotent cells as well as the expansion of the differentiating CMs (*46*). We and others have previously demonstrated that matPGDM-

exposed embryos display a reduction in CM proliferation in E13.5 hearts as measured by the number of PHH3^{+} and BrdU^{+} cells respectively (*26, 30*). Here, we show that this defect in cellular proliferation can be traced back to differential gene expression in earlier stages of heart development. DEG analysis on CM subclusters at E9.5 and E11.5 show genes and pathways critical for cell proliferation are perturbed due to matHG. To assess the impact of this cell-cycle gene expression on proliferation, we evaluated the percentage of mitotic cells. We used E9.5 and E11.5 *wt* and *Rosa*$^{mTmG/+}$ hearts to co-immunostain either Tnnt2 or GFP and PHH3(Ser10), a mitosis maker. At E9.5, the percentage of mitotic cells in low- and high matHG-exposed E9.5 did not reach statistical significance. We did note a decrease in PHH3+ CMs suggesting a trend towards decreased CM proliferation (**Fig. S7A-C, G**). In contrast, CM proliferation was found to be significantly downregulated in E11.5 embryos in a dose-dependent manner when compared to CNTRL embryos (**Fig. S7D-G**). To assess the specific impact of matHG on the proliferation of SHF-CMs, similar experiments were performed in *Is1l-Cre*$^{+}$*; Rosa*$^{mTmG/+}$ embryonic hearts. We found that GFP+PHH3+ cells were markedly diminished at both E9.5 and E11.5. This data indicated that embryonic cardiomyocytes are most sensitive cell type when exposed to a matHG environment (**Fig. S7H-P**). Gene-expression-based cell cycle scoring analysis (*47*) in our scRNAseq data further showed that in matHG, a lower proportion of cells are in the S/G2/M phases of the cell cycle compared to CNTRL embryos (**Fig. SQ**). We further checked the transcriptomic profile of cell-cycle genes (*Mki67, Ccnd2,* and *Ccnd1*) in different CM subclusters using E9.5 and E11.5 scRNA-seq data. This analysis showed that in E9.5 and E11.5 AVC-CMs, fewer cells are expressing *Ccnd2* and *Ccnd1* while

their expression was downregulated in E11.5 Atr- and Ven-CMs under matHG (**Fig. S7R**). However, no obvious difference in *Mki67, Ccnd2,* and *Ccnd1* expressions was observed in matHG-exposed E9.5 OFT and Ven-CM. Together, our lineage tracing studies corroborated the scRNA-seq results and show that the *Isl1*$^{+}$-SHF-cells response to matHG environment results in defective CM differentiation and contributes to reduced proliferation.

The *Isl1*-gene regulatory network is perturbed in response to matHG

To gain insight into HG-mediated changes in the *Isl1*-dependent gene regulatory network (Isl1-GRN) during cardiogenesis, we reconstructed a protein-protein interaction map using String database. We identified a list of pioneer TFs and epigenetic modifiers previously known to function as part of an Isl1-dependent core network for RV and OFT development (**Fig. 7A**). Using scRNA-seq data, we detected significant changes ($P_{adj} < 0.05$) in the expression of *Isl1*, *Mef2c, Id2, Pdgfra, Pitx2, Mpped2, Foxp1, Crabp2, Tgfbi, Irx3, Bmpr2, Hes1* in E9.5 SHF cells with matHG (**Fig 7B**). There is evidence to support that these cardiac TFs individually or in combination with epigenetic modulators regulate SHF development and appeared to affect the expansion of myocardial cells (*24, 31, 48, 49*). To test the prediction of Isl1-GRN perturbations *in vivo*, we focused on two specific candidates, Hand2 and Nkx2-5. Their expression was examined in CNTRL vs. matHG-exposed *Isl1-Cre*$^{+}$*; Rosa*$^{mTmG/+}$ E9.5 hearts. Immunostaining with Hand2 and GFP revealed downregulation of Hand2 expression in matHG-exposed E9.5 distal OFT (**Fig 7C-H**). Of note, Nkx2-5^{+}GFP^{+} expression was affected in the RV, suggesting that matHG

triggers the specification of chamber myocardium (**Fig 7I-N**). A recent scRNA-seq study showed the failure of OFT-CM specification in *Hand2*-null embryos, whereas RV myocardium was shown to be specified but failed to properly differentiate and migrate (*31*). Other studies demonstrate that *Nkx2-5* is required for SHF proliferation through suppression of Bmp2/Smad1 signaling and negatively regulates *Isl1* expression (*49, 50*). Therefore, dysregulation of Hand2 and Nkx2-5 expression in *Isl1*$^{+}$ SHF-cells suggest underlying OFT and septation defects in the matHG-exposed embryonic hearts. In summary, we proposed a "maternal teratogen-induced CHD model", in which matHG perturbs Isl1-GRN in the SHF progenitors, leading to impaired CM differentiation and increases the risk of CHD (**Fig 7O**).

Discussion:

In this study we report two key findings. First, we demonstrated a dose-response relationship between maternal hyperglycemia and severity of CHD phenotypes by detailed characterization of embryonic hearts at multiple developmental time points during cardiac morphogenesis. Second, we have segregated the cardiac cellular responses to maternal hyperglycemia using an *in vivo* single cell transcriptomics approach. We further extended the computational reconstruction of differentiation trajectories to demonstrate that the matHG environment during early stages of heart development alters the transcriptional network in *Isl1*$^{+}$ SHF cells and CM subpopulations. Using cell-fate mapping studies in the matHG background, we were able to confirm that the *Isl1*$^{+}$ SHF-progenitor population are susceptible to matHG exposure and this leads to impaired CM

differentiation. In summary, the molecular interactions of Isl1-GRN inferred from single-cell expression data suggest its regulatory role in matPGDM induced CHD.

CHD-causing genes are well studied in murine heart development. Studies have shown that complete deletion of causative genes results in embryonic lethality while heterozygous mice are often unaffected (*51, 52*). Recently, disease modeling of *GATA4, TBX5* pathogenic variants in human iPSC-derived cardiomyocytes and iPSCs-derived endothelial cells from patients with BAV and CAVD with *NOTCH1* haploinsufficiency have predicted that CHD-linked gene regulatory network is sensitive to the gene dosage (*53-55*). These studies strongly suggest that cell type and gene-dosage is critical for normal cardiac development. Like gene dosage, the impact of teratogenic dose is also of high clinical significance. The variability in the adverse maternal hyperglycemic environment in presence or absence of genetic variants could impact the disease penetrance and contribute to phenotypic severity observed in CHD patients. The clinical manifestations of matPGDM-induced CHD are variable. Among them, infants born with VSD, conotruncal malformations and heterotaxy are significantly higher in mothers with PGDM (*13, 56*). However, these studies fail to differentiate between the contribution of the genetic variants and that of the maternal environment linked to CHD. The primary teratogen in all human diabetic pregnancies is hyperglycemia. Additional studies using ex vivo and avian models have confirmed that matHG is the primary teratogen in inducing cardiac defects (*56, 57*). With the help of the experimental model of matPGDM, we and others have established a gene-environment interaction model and recapitulated the increased rate of matHG-

induced CHD both in presence of *wt* (this study) and haploinsufficient cardiac genes (*10, 26, 27*). More mechanistic studies are needed to identify HG-sensitive cardiac regulatory genes, the spatiotemporal requirement in FHF, SHF, cardiac NC cell lineages and mode of action in response to matHG. Our *in vivo* studies with *wt* embryonic hearts led us to compare the cardiac phenotypes that occur under the direct influence of an HG environment. We examined E9.5, E11.5 and E13.5 embryonic hearts to understand the effect of low and high levels of matHG when they undergo key events during cardiogenesis. Here, E9.5 matHG-exposed embryos mostly showed myocardial thinning and trabeculation defects. Whereas, E11.5 and E13.5 exhibited RV and LV wall thinning and higher incidence of VSD. Defects in trabeculation, ventricular wall compaction therefore indicate failure of myocardial maturation under an HG environment. However, E15.5 embryos exhibited VSD, semilunar valve thickening and truncus arteriosus when exposed to matHG. In a subset of these embryos, we also noticed an increased occurrence of ventricular hypertrophy, which is also observed with maternal gestational diabetes. Therefore, it remains critical to evaluate the acute vs. chronic effect of matHG at later stages of gestation, where the mechanism is related to fetal hyperinsulinemia and increased expression of insulin receptors which could lead to proliferation and hypertrophy of CMs (*58, 59*).

The complexity of cardiac phenotypes in early-stage embryos suggests heterogeneity in the cellular response to matHG. Seminal studies in human and mouse models have profiled the transcriptomes of single cells during normal cardiovascular

development at an unprecedented resolution to reveal progenitor cell specification and their fate choice (*60-63*), but the toxicity of HG on these cardiac cell lineages remains undefined. Using *in vivo* scRNA-seq technology, we uncovered transcriptional differences in CNTRL vs. matHG-exposed E9.5 and E11.5 hearts. These two time points were chosen to understand the molecular differences underlying matHG-exposed phenotypes described earlier. We captured MP, CM, EC, FM, EP and NC in E9.5 and E11.5 hearts and have shown differences in cellular transcriptional response to matHG. Based on the clinical manifestation of CHD in the infants of PGDM mothers or dams, we demonstrate that a population of Isl1^{+} cells which forms SHF is sensitive to HG exposure. We focused on SHF-cells marked by *Isl1*, which primarily contribute to the OFT, RV and parts of the atria, where its expression is regulated as the cells adopt a differentiated phenotype (*64*). In human studies, loss-of-function variants in *ISL1* were shown to contribute to CHD and dilated cardiomyopathy alone or in synergy with *MEF2C*, *TBX20* or *GATA4* (*65*). While mutations in this gene were also found to be associated with maturity-onset diabetes of the young and type 2 diabetes (*65, 66*). In this study, we demonstrated that the *Isl1*$^{+}$ MP and *Tnnt2*$^{+}$ CM subjected to matHG have the most significant differences in gene-expression among other cell types. Reclustering and pseudotemporal ordering of the MP-CM clusters reveal the altered distribution of BMP, SHF and OFT, AVC, Ven and Atr-CM subpopulations in matHG-exposed hearts compared to controls. Notably, matHG-induced higher expression of *Isl1* in myogenic progenitors of branchial arches and a reduction in anterior heart field cells and suggest that dysregulation of these precursors cells and their derivatives lead to OFT and septation defects. To validate if the SHF-derived CMs are

HG-sensitive, and that CM differentiation is affected, we showed a reduction in *Isl-1*-derived *Tnnt2*$^{+}$ cells in E9.5, E11.5, and E13.5 *Isl1-Cre*$^{+}$*; Rosa*$^{mt/mG}$ embryonic hearts when exposed to matHG. In parallel, we also recapitulated CM proliferation defects in *wt* and *Isl1*$^{+}$SHF-CMs at E9.5 and E11.5 as previously described in E13.5 embryos (*26*). In the end, we found that chamber myocardium vs. OFT and AVC-CM show clear patterning differences, both in terms of transcriptional response and biological processes which define its function. One limitation of this scRNA-sequencing is that it was performed after pooling multiple embryonic hearts exposed to high-matHG and compared with CNTRL embryonic hearts. Since our group and others have shown PGDM-induced CHD occurs in ~10-50% *wt* embryos depending on matHG dosage, it suggests we are not observing transcriptional differences from genes with subtle changes.

Maternal hyperglycemia is a teratogen and exerts a pleotropic effect on multiple cell-types. In addition to cardiomyocytes and their precursors, we checked differences in gene expression in non-myocardial cell-lineages. DEG analysis in EC, FM, EP, and NC clusters also revealed significant changes in the extracellular matrix organization, angiogenesis and tube formation, OFT morphogenesis and heart valve development (**Fig. S8A-I and Fig. S9A-G**). Importantly, EC-FM specific genes including *Notch1, Klf4, TGFβ, Snai2, Sox9, Vcan, Twist2, Pdlim3, Gata6, Bmp4, Msx1, Pax3* were previously shown to be dysregulated with matHG exposure that contributes to abnormal EndoMT, mesenchymal cell differentiation, and migration of cardiac NC cells (*17, 26, 30*). Reduced proportion of FM cells in response to matHG showed concomitant downregulation of

EndoMT genes such as, *Vcan Sox9, Postn,* and Bmp/Tgfβ signaling (**Fig. S8E-I**) This aberrant gene expression profile in EC-FM cells corroborate the underlying cause of endocardial cushion defects seen in diabetic pregnancies (*17*). In the *Tbx18*$^{+}$ EP cluster, we found the expression of *Wt1, Dcn,* and *Upk3b* were significantly downregulated with matHG and Wnt inhibitor, *Sfrp1* was upregulated at E9.5 (**Fig. S9E**) indicating migratory defects in proepicardial derived mesothelial cells. We also show matHG reduced the protein expression of Fn1 in E13.5 embryos (**Fig. S9F**). Studies have shown that EP-EMT is followed by activation of Fn1 necessary for ECM production and migration during heart development (*67*). Therefore, altered gene expression in EP cells suggests that matHG possibly affects the delamination and migration process of a subset of proepicardial and EMT-derived cells that invade the myocardium to generate the majority of vascular smooth muscle cells and cardiac fibroblasts in the heart to perturb Ven-CM maturation (49). Finally, we noticed an enriched expression of *Dlx2, Dlx5* only at the E9.5 NC cluster, but a marked reduction in E11.5 under matHG exposure (**Fig. S9E-G**). Recent scRNA-seq on E8.5-E10.5 *Wnt1*^{Cre}*/R26R*^{Tomato} mouse embryos highlight the branching trajectory of differentiating NC cells, where expression of *Dlx6* is followed by activation of *Msx2*, *Hand2*, and other cardiac markers such as *Hand1* and *Gata6* (*68*). This data implies that long-range inductive signals for NC cells could compensate for the deficits in EndoMT-derived cells in the OFT as a result of HG-mediated toxicity. The misallocation of mesenchymal cells of NC origin could lead to valvular defects seen later in the gestation.

Future mechanistic studies are needed to evaluate the epigenetic basis of Isl1-GRN underlying matHG dosage and their progenitor-specific role in regulating CM differentiation (**Fig 7O**). In this study, we characterized the embryonic response to matHG by establishing the interaction between environmental dosage and CHD severity. While scRNA-seq uncovered distinct cell type-specific responses to matHG underlying the pathogenesis, more work is required to test their causality. These differentially expressed genes in each individual cluster would serve as potential candidates to study gene-environment interaction and facilitate the development of new therapeutics to mitigate PGDM-induced CHD.

Figures and figure legends:

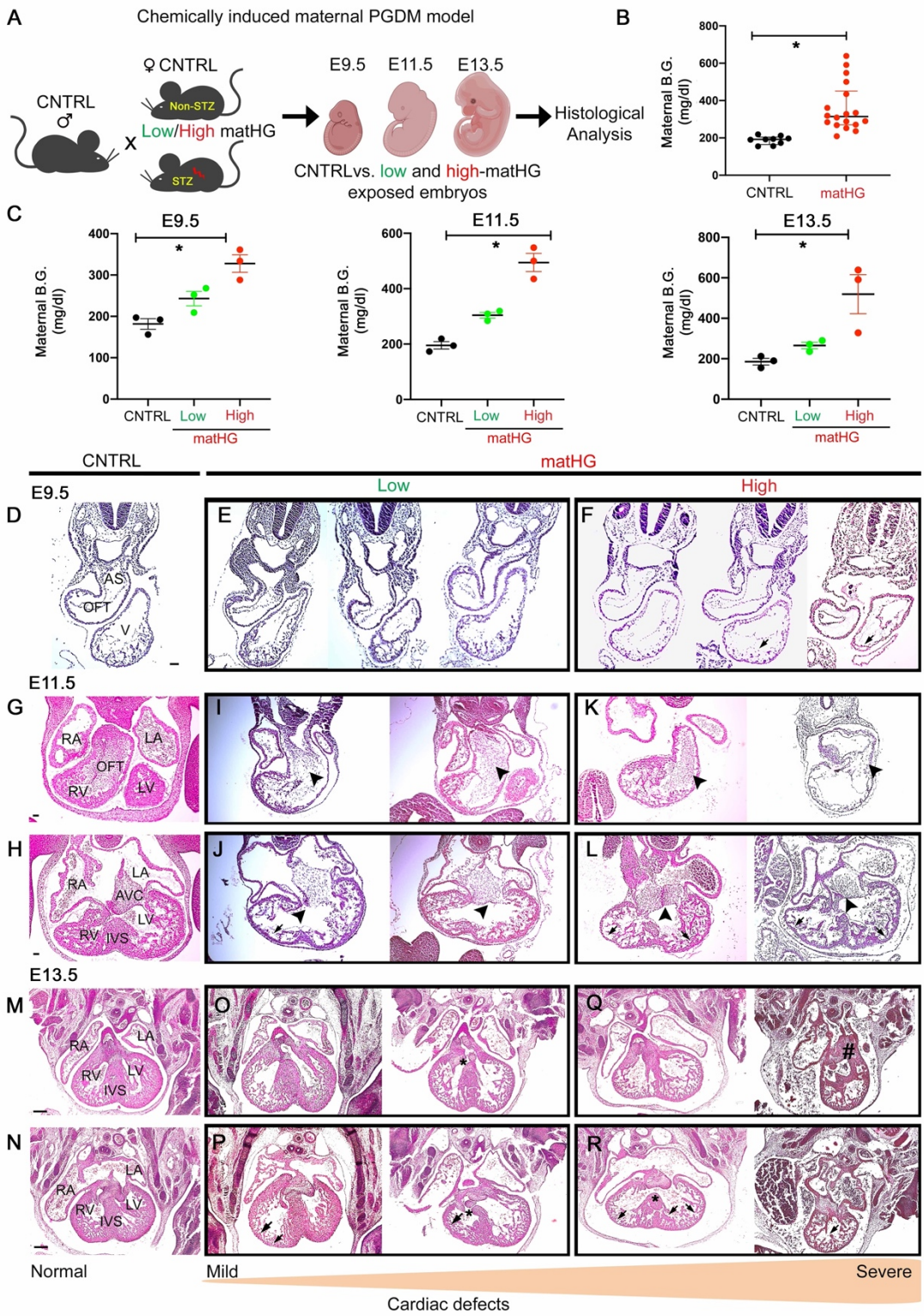

Figure 1

Fig. 1. Dose-dependent phenotypic severity of matHG-induced CHD phenotypes

(A) Schematic representing breeding scheme (made in ©BioRender) of a chemically induced murine model of pregestational diabetes (PGDM) exhibiting maternal hyperglycemia (matHG). Control (CNTRL) males bred with streptozotocin (STZ)-treated and non-STZ-treated CNTRL C57BL/6J females, and E9.5, E11.5 and E13.5 embryos were analyzed. **(B)** Distribution of maternal blood glucose (B.G.) levels in CNTRL (n=9) vs. matHG-exposed (n=18) litters. **(C)** Maternal B.G. levels in STZ-treated females in low matHG and high-matHG groups compared to CNTRL females. **(D-R)** Representative transverse sections of CNTRL (**D, G, H, M and N**) and matHG-exposed embryonic hearts stained with hematoxylin and eosin show dose-dependent phenotypic severity of CHD at E9.5 **(**panels **E, F)**, E11.5 **(**panels **I-L)** and E13.5 **(**panels **O-R)** when subjected to low- and high-matHG**.** Trabeculation defects and ventricular wall thinning was found at all time points **(**arrows in **F, J, L, P, R)**, At E11.5, hypocellular outflow tract (OFT) and atrioventricular canal (AVC) endocardial cushion defects **(**arrowheads in **I-L)** were seen. A poorly formed interventricular septum (IVS) **(**panels **J, L, Q, R)** and ventricular septal defects **(**asterisks in panels **O, P, R)** in E11.5 and E13.5 embryos exposed to low and high-matHG were also identified. # in **(Q, R)** indicates double outlet right ventricle (DORV) in E13.5 embryos exposed to high-matHG. V, ventricle, RA, right atrium, LA, left atrium; RV, right ventricle; LV, left ventricle. Scale bars: 200µm. Three independent litters per developmental time point were used for embryo collection and phenotypic analysis Data presented as mean ± SEM. Statistics comparisons made between maternal B.G. levels

in CNTRL vs. matHG-groups using unpaired Student's *t*-test and one-way ANOVA with Bonferroni's multiple test correction. * indicates 2-tailed p-value <0.05.

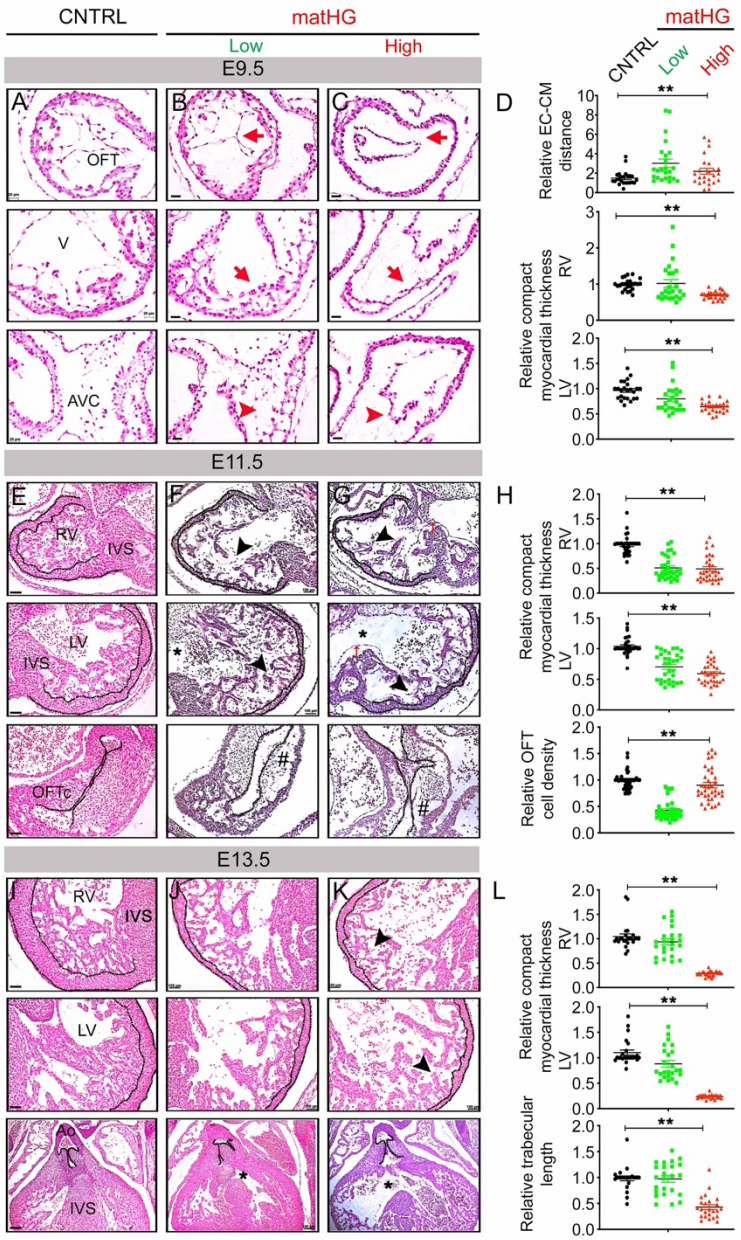

Figure 2

Fig. 2. Effect of maternal hyperglycemic dosage on outflow tract (OFT) and ventricular morphogenesis

(A-C) Representative high magnification histological images from low and high matHG-exposed E9.5 hearts show myocardial wall thinning (red arrows), trabeculation and touchdown defects with increased endothelial-myocardial (EC-CM) distance and impaired atrioventricular canal (AVC) development **(**red arrowheads **in B, C)** compared to CNTRL hearts **(A)** and quantified in **D**. **(E-G)** Representative histological images of E11.5 hearts show dose-dependent RV and LV wall thinning (black dotted lines), trabeculation defects (black arrowheads), increased EC-CM distance (red arrows), poorly formed interventricular septum (IVS) with ventricular septal defects (indicated by *) and reduced cell density in the OFT (indicated by #) in response to low and high-matHG exposure **(F, G)** compared to CNRTL E11.5 embryos **(E)**. Quantification of embryonic RV and LV wall thickness and OFT cell density between CNTRL and HG groups are shown in **H**. **(I-K)** Low and high-matHG-exposed E13.5 embryos displayed thin RV and LV wall thinning (black dotted lines), shorter trabecular length (black arrowheads), VSD and overriding aorta (indicated by *) when compared to CNTRL E13.5 embryos **(I)**. Quantification between groups is shown in **L**. $n \geq 3$ embryos/group. Data presented as mean ± SEM. ** indicates two-tailed p-value < 0.05 after one-way ANOVA analysis with Bonferroni correction. Scale bars (A-C: 200µm; D-I:500µm, J-L: 20µm, N-P: 50µm and R-T: 100µm).

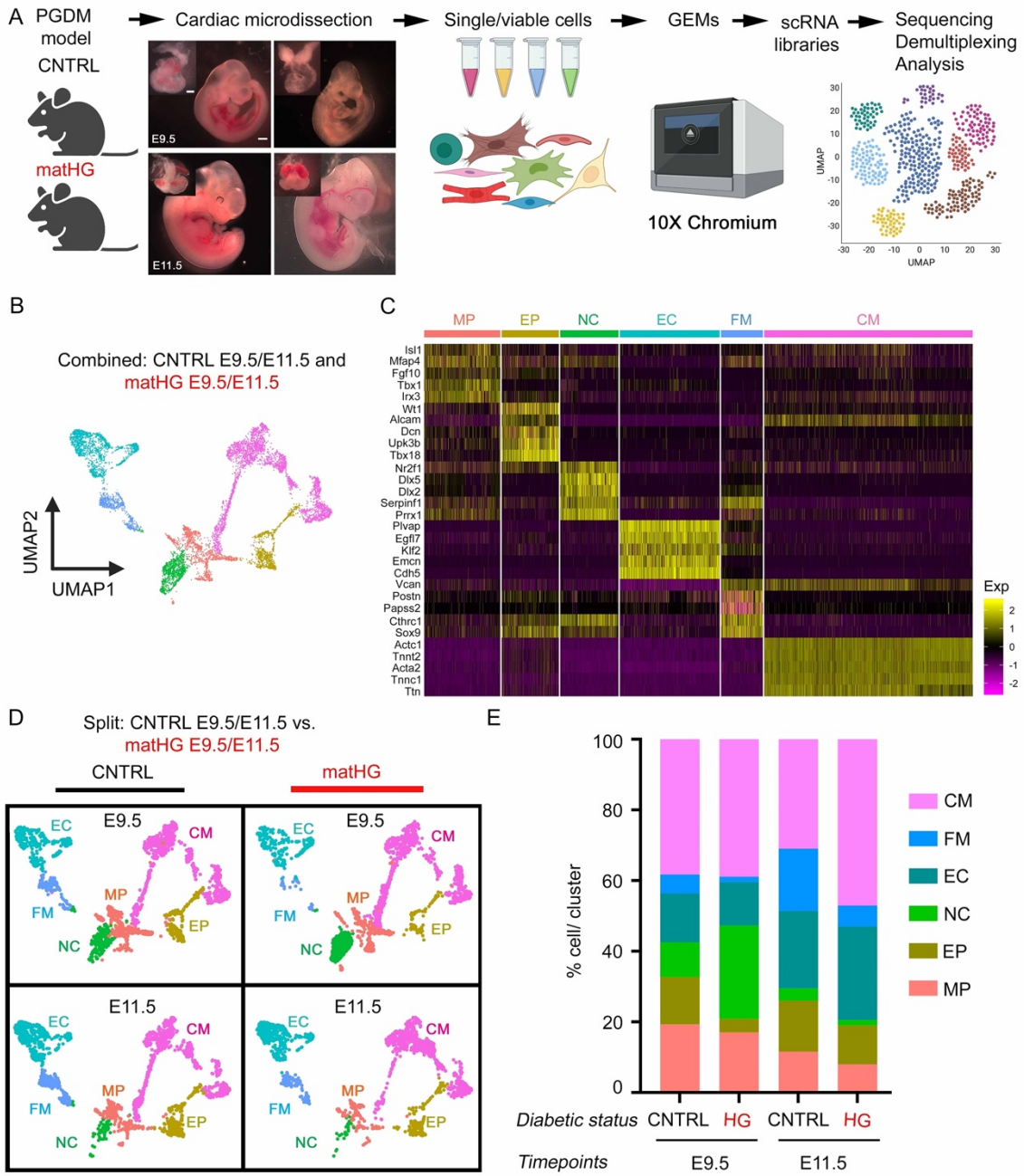
A
PGDM model
CNTRL
matHG
Cardiac microdissection
E9.5
E11.5
Single/viable cells
GEMs
10X Chromium
scRNA libraries
Sequencing
Demultiplexing
Analysis
UMAP
B
Combined: CNTRL E9.5/E11.5 and
matHG E9.5/E11.5
UMAP2
UMAP1
C
MP
EP
NC
EC
FM
CM
Isl1
Mfap4
Fgf10
Tbx1
Irx3
Wt1
Alcam
Dcn
Upk3b
Tbx18
Nr2f1
Dlx5
Dlx2
Serpinf1
Prrx1
Plvap
Egfl7
Klf2
Emcn
Cdh5
Vcan
Postn
Papss2
Cthrc1
Sox9
Actc1
Tnnt2
Acta2
Tnnc1
Ttn
Exp
D
Split: CNTRL E9.5/E11.5 vs.
matHG E9.5/E11.5
CNTRL
matHG
E9.5
E11.5
EC
CM
FM
MP
NC
EP
E
% cell/ cluster
Diabetic status
CNTRL
HG
Timepoints
E9.5
E11.5

Figure 3

Fig. 3. Single-cell transcriptomic profiling in E9.5 and E11.5 hearts reveals a heterogenous response to maternal hyperglycemia

(A) Experimental pipeline for tissue collection, dissociation, single-cell preparation, 10X library generation and sequencing of E9.5 and E11.5 hearts exposed to CNTRL environment (blood glucose <200 mg/dl) and matHG (blood glucose >300 mg/dl). The diagram made in ©BioRender. **(B)** Total 8503 single cell transcriptomes were utilized for comparative analysis between developmental stages and matHG status. Uniform Manifold Approximation and Projection (UMAP) plot displays distribution of six broadly classified cardiac cell populations combined from E9.5 and E11.5 hearts subjected to CNTRL or matHG environment. Each dot represents an individual cell and cluster identities are colored. **(C)** An expression heatmap of the top five marker genes of six cardiac populations is shown, where rows indicate each marker gene and columns denote single cells. MP= multipotent progenitor, EP=epicardial, NC=neural crest, EC=endocardial/endothelial, FM=fibromesenchymal and CM=cardiomyocytes. **(D)** After marker identification and classification, four UMAP plots were generated to demonstrate CNTRL and matHG-exposed cells in each cluster at E9.5 and E11.5. **(E)** Bar graphs represent the distribution of each cluster (in percentages) normalized to the total number of cells per sample and reveal differences due to matHG exposure at E9.5 and E11.5. Cluster identities are indicated in colors.

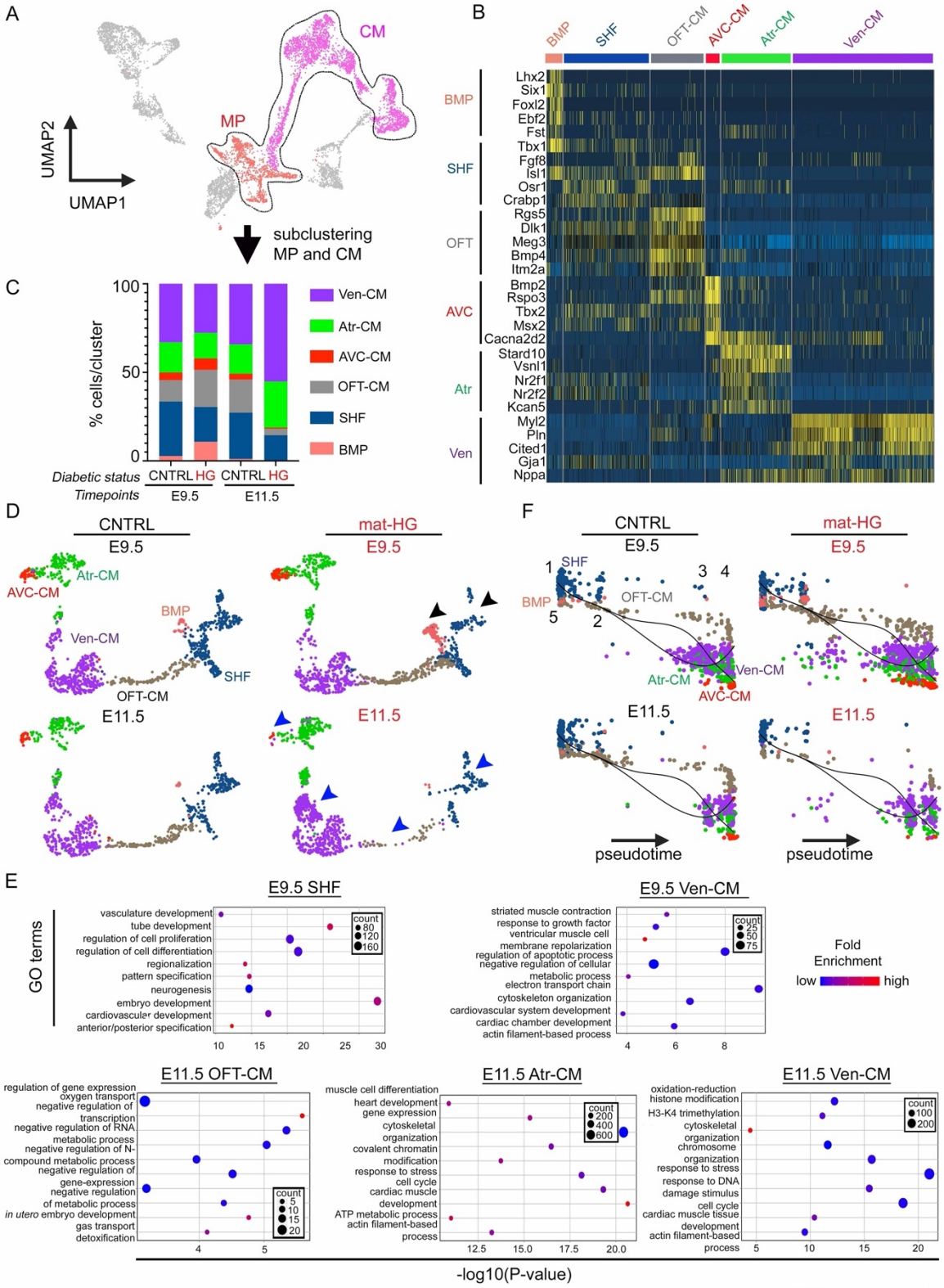
A
CM
MP
UMAP2
UMAP1
subclustering
MP and CM
B
BMP
SHF
OFT-CM
AVC-CM
Atr-CM
Ven-CM
Lhx2
Six1
Foxl2
Ebf2
Fst
Tbx1
Fgf8
Isl1
Osr1
Crabp1
Rgs5
Dlk1
Meg3
Bmp4
Itm2a
Bmp2
Rspo3
Tbx2
Msx2
Cacna2d2
Stard10
Vsnl1
Nr2f1
Nr2f2
Kcan5
Myl2
Pln
Cited1
Gja1
Nppa
C
% cells/cluster
Diabetic status
CNTRL HG CNTRL HG
Timepoints
E9.5
E11.5
D
CNTRL
mat-HG
E9.5
E11.5
F
pseudotime
E
E9.5 SHF
E9.5 Ven-CM
E11.5 OFT-CM
E11.5 Atr-CM
E11.5 Ven-CM
GO terms
Fold Enrichment
low
high
-log10(P-value)

Figure 4

Fig. 4. Subclustering and pseudotime ordering of MP-CM cluster show differential response to maternal hyperglycemia

(A) Multipotent progenitor or MP (1194 cells; 14.1%) and cardiomyocytes or CM (3273 cells; 38.5%) cells were reclustered after combining CNTRL and high-matHG exposed E9.5 and E11.5 single cell transcriptomes implemented in Seurat. **(B)** Expression heatmap represents cluster-specific the top 5 marker gene expression. Rows indicate each marker gene and columns denote single cells. Based on marker gene expression, MP cells are broadly classified into anterior/posterior second heart field (SHF) and branchiomeric muscle progenitors (BMP). Subclustering of CMs reveals outflow tract (OFT), atrioventricular canal (AVC), atrial (Atr) and ventricular (Ven) cardiomyocytes. **(C)** Bar graphs represent the distribution of each cluster (in percentages) normalized to the total number of cells per sample and reveal differences relative to matHG exposure at E9.5 and E11.5. Cluster identities are indicated in colors. **(D)** Split UMAP plots show spatiotemporal and matHG specific changes in CM subpopulations. Each dot represents an individual cell and is colored by its respective subcluster identities in the UMAPs. Marked changes in SHF and BMP (black arrowheads) at E9.5 and SHF, OFT, Atr- and Ven-CMs (blue arrowheads) in E11.5 embryos are denoted. **(E)** The enriched (FDR $\leq$ 0.05) gene ontology (GO) terms associated with HG-sensitive, differentially expressed genes (DEGs) in E9.5 SHF and Ven-CM and E11.5 OFT, Atr and Ven-CM subclusters are displayed in bubble plots (GO-term on the y axis and fold enrichment score on the x-axis). The count represents gene number, also indicated by circle size. whereas the color denotes the up (red) or downregulation (blue) of the specific GO term in the sample. **(F)**

Single-cell trajectory analysis on combined MP-CM was performed using Monocle 2 and Slingshot. Five cell states (state 1- 5) were identified and shown in two-dimensional Slingshot images. Each dot represents an individual cell and is colored by its respective subcluster identities across the pseudotime. The black line indicates direction of the trajectory.

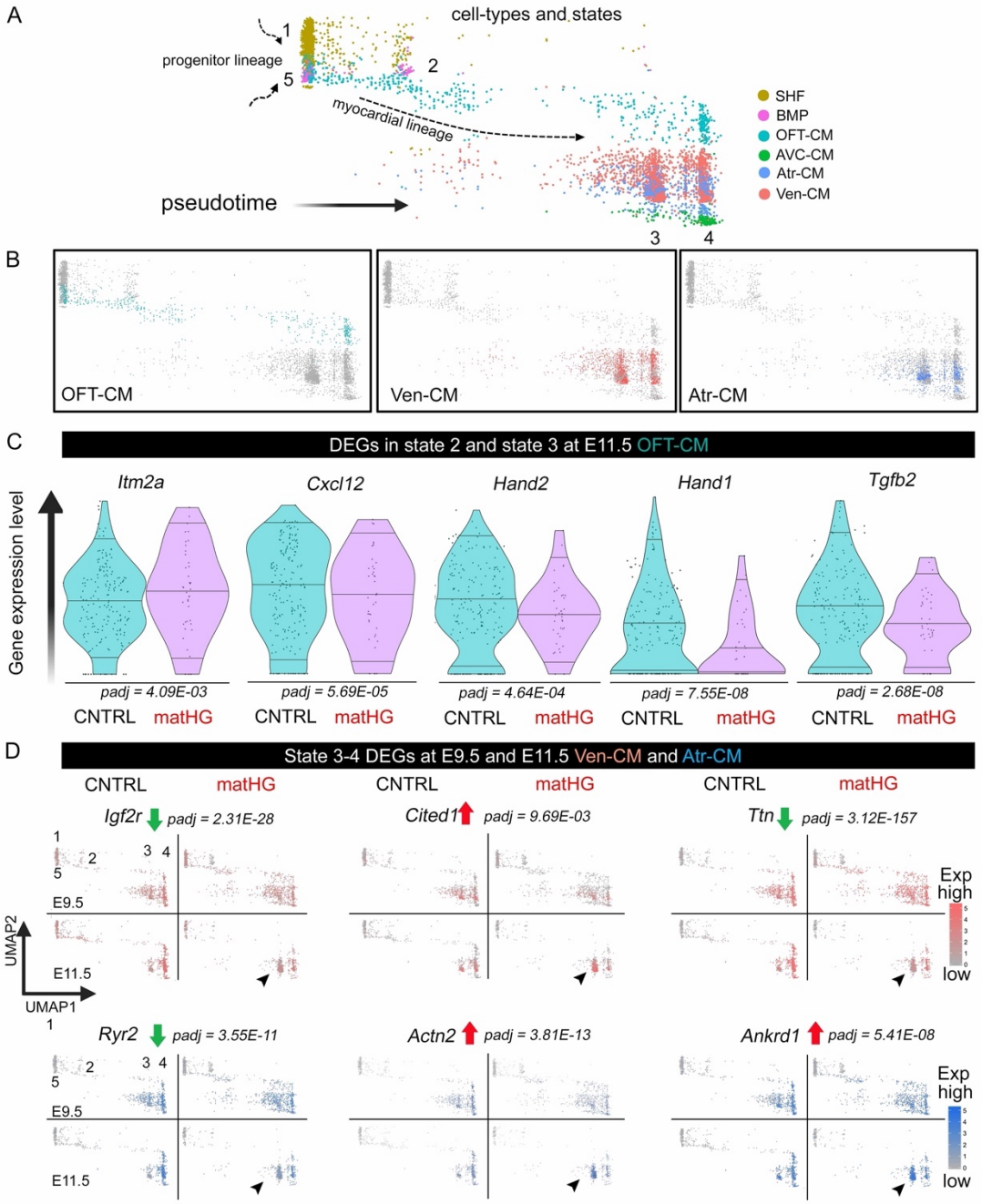
A
cell-types and states
progenitor lineage
1
2
5
myocardial lineage
pseudotime
3
4
SHF
BMP
OFT-CM
AVC-CM
Atr-CM
Ven-CM
B
OFT-CM
Ven-CM
Atr-CM
C
DEGs in state 2 and state 3 at E11.5 OFT-CM
Gene expression level
Itm2a
Cxcl12
Hand2
Hand1
Tgfb2
padj = 4.09E-03
padj = 5.69E-05
padj = 4.64E-04
padj = 7.55E-08
padj = 2.68E-08
CNTRL
matHG
D
State 3-4 DEGs at E9.5 and E11.5 Ven-CM and Atr-CM
CNTRL
matHG
Igf2r
padj = 2.31E-28
Cited1
padj = 9.69E-03
Ttn
padj = 3.12E-157
E9.5
E11.5
UMAP2
UMAP1
Exp
high
low
Ryr2
padj = 3.55E-11
Actn2
padj = 3.81E-13
Ankrd1
padj = 5.41E-08

Figure 5

Fig. 5. Exposure to maternal hyperglycemia disrupts CM differentiation

(A) Pseudotime trajectory of progenitor and myocardial lineages from CNTRL and HG-exposed E9.5 and E11.5 hearts identify 5 pseudotime states, labelled 1 – 5. Cluster identities are colored and defined in key. **(B)** The distribution of OFT (state 2), Ven and Atr-CMs (states 3 and 4) are shown in isolated pseudotime plots. **(C)** Violin plots show statistically significant (p_{adj} <0.05) gene expression differences in *Itm2a, Cxcl12, Hand2, Hand1* at state 2 and *Tgfβ2* at state 3 OFT-CMs at E11.5. **(D)** UMAP feature plots at E9.5 and E11.5 show state 3 and state 4 Ven-CM and Atr-CM, respectively. Differential gene expression of *Igf2r, Cited1, Ttn, Ryr2, Actn2* and *Ankrd1* are denoted by p_{adj} <0.05. Each dot represents single cells and color intensities denote gene expression levels. Up or downregulation of myocardial maturation genes are indicated by red and green arrows, respectively. Black arrowheads indicate state 3 as low-*Ttn*$^{+}$; less differentiated CM subpopulations than state 4. OFT= outflow tract, Ven = ventricular and Atr = atrial.

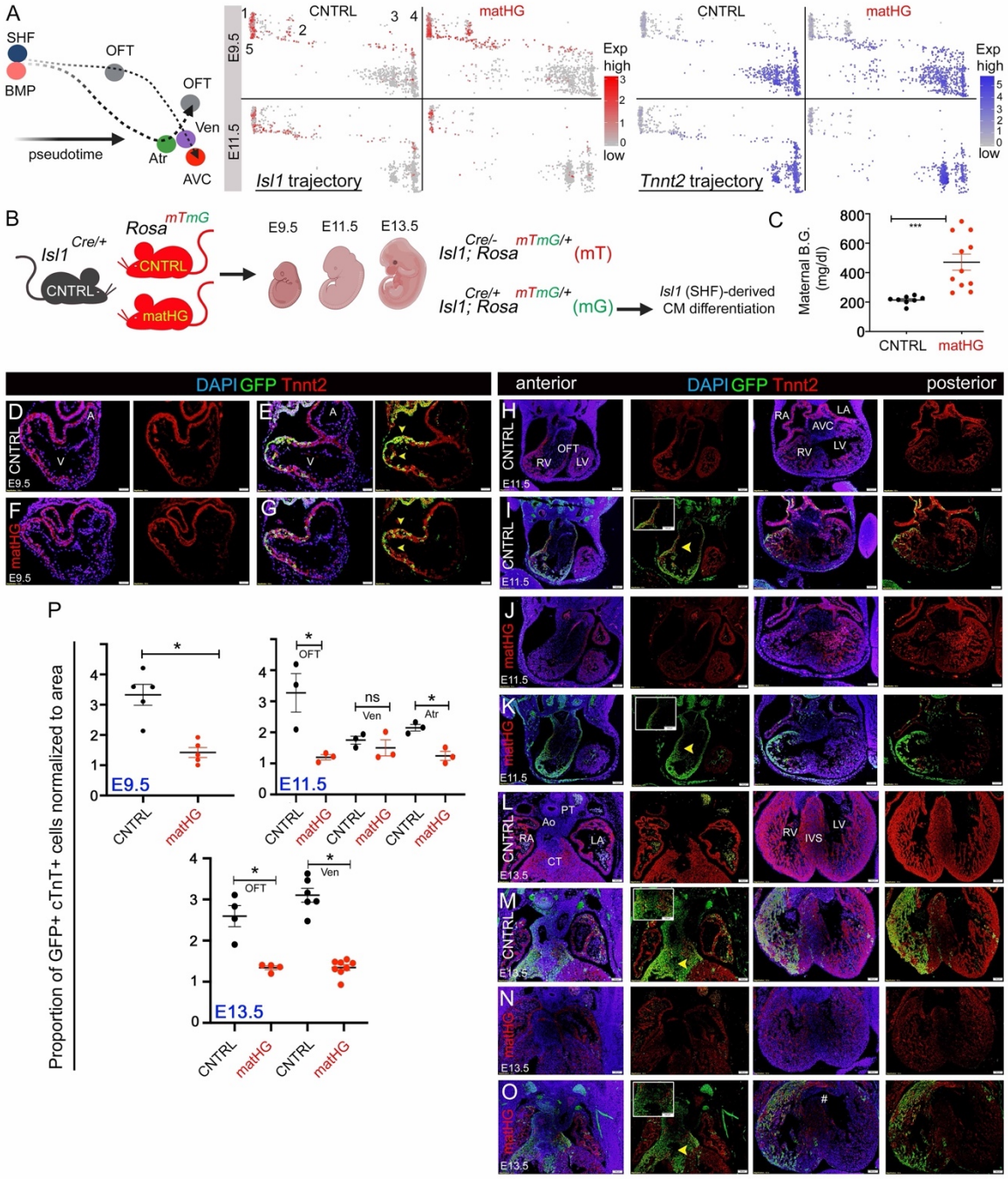
A
SHF
BMP
OFT
OFT
Ven
Atr
AVC
pseudotime
E9.5
E11.5
CNTRL
matHG
Isl1 trajectory
Tnnt2 trajectory
Exp high
low
B
Isl1 Cre/+
Rosa mTmG
CNTRL
matHG
E9.5
E11.5
E13.5
Isl1; Rosa Cre/- mTmG/+ (mT)
Isl1; Rosa Cre/+ mTmG/+ (mG)
Isl1 (SHF)-derived CM differentiation
C
Maternal B.G. (mg/dl)
CNTRL
matHG
DAPI GFP Tnnt2
anterior
posterior
P
Proportion of GFP+ cTnT+ cells normalized to area
E9.5
E11.5
E13.5
OFT
Ven
Atr
ns

Figure 6

Fig. 6. Maternal hyperglycemia impedes SHF-derived cardiomyocyte differentiation *in vivo*

(A) Lineage map of SHF and myocardial subpopulations. Feature plots of SHF-marker *Isl1* and cardiac muscle marker *Tnnt2* at E9.5 and E11.5 hearts in the setting of control (CNTRL) vs. matHG show changes in expression across pseudotime states 1-5. Each dot represents single cells and color intensity denotes gene expression levels. **(B)** The schematic diagram indicates *in vivo* characterization of SHF-lineage specific response to matHG. *Isl1-Cre*$^{+/-}$ males bred to CNTRL and STZ-treated matHG *Rosa*$^{mT/mG}$ reporter females and E9.5, E11.5 and E13.5 embryos are collected for molecular analysis. **(C)** The distribution of maternal B.G. levels in CNTRL (n=8 litters) vs. matHG (n=11 litters) mice are shown. **(D-O)** Co-immunofluorescence staining shows Tnnt2^{+} CMs (red) and *Isl1*-derived GFP^{+}Tnnt2^{+} CMs (i-CMs, in yellow) in *Isl1Cre*$^{-}$*; Rosa*$^{mTmG/+}$ and *Isl1Cre*$^{+}$*; Rosa*$^{mTmG/+}$ littermates in E9.5 **(D-G)**, E11.5 **(H-K)** and E13.5 **(L-O)** hearts between CNTRL and matHG, where yellow arrowheads indicate differentiated CMs derived from *Isl1*$^{+}$ SHF-lineage. (**I, K, M, O**) GFP^{+}Tnnt2^{+} CMs in embryonic hearts (from anterior to posterior direction) show perturbed CM differentiation with matHG exposure (yellow arrowheads). White insets in **I', K', M'** and **O'** show high magnification images of GFP^{+}Tnnt2^{+} CMs in **I, K, M, O**. MatHG-exposed E13.5 embryos demonstrated a thin myocardial wall, impaired trabeculation and ventricular septal defect (white hashtag). **(P)** The proportion of GFP^{+}Tnnt2^{+} iCMs in outflow tract (OFT), atrial (Atr) and ventricular (Ven)-CM normalized to myocardial area are quantified ($n \geq 3$) and compared between CNTRL and matHG-exposed E9.5, E11.5 and E13.5 *Isl1Cre*$^{+}$*; Rosa*$^{mTmG/+}$ embryos.

Nuclei stained with DAPI are in blue. A, atria; V, ventricle; LV, left ventricle; RV, right ventricle. Data presented as mean ± SEM; Statistical comparisons made between CNTRL and matHG groups using unpaired Student's *t*-test. * indicates p-value < 0.05. Scale bars: 50µm (D-G) and 100µm (H-O). The images (A, B) are made in ©BioRender.

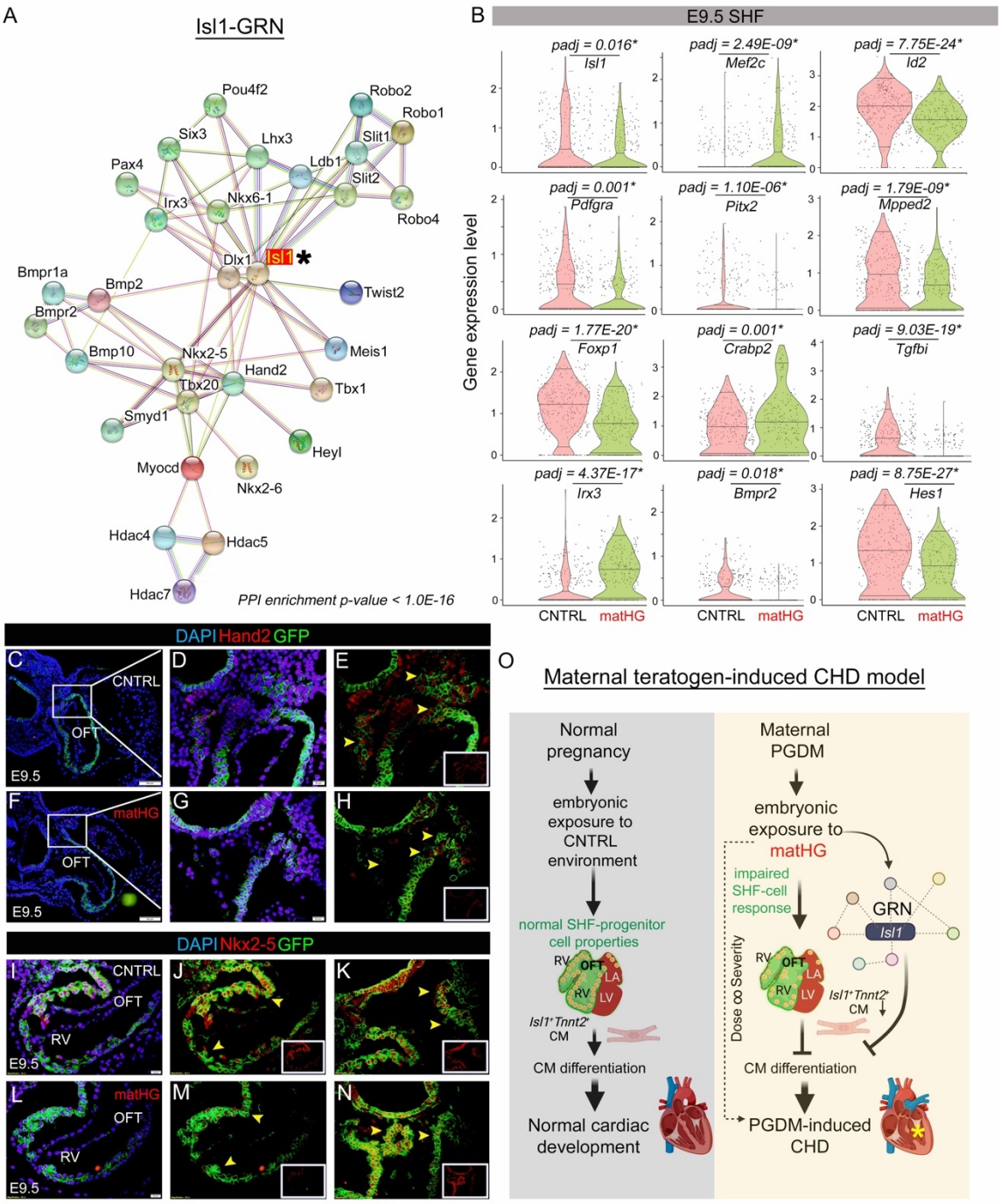
A
Isl1-GRN
Pou4f2
Robo2
Robo1
Six3
Lhx3
Slit1
Pax4
Ldb1
Slit2
Irx3
Nkx6-1
Robo4
Dlx1
Isl1
Bmpr1a
Bmp2
Twist2
Bmpr2
Bmp10
Nkx2-5
Meis1
Hand2
Tbx20
Tbx1
Smyd1
Heyl
Myocd
Nkx2-6
Hdac4
Hdac5
Hdac7
PPI enrichment p-value < 1.0E-16
B
E9.5 SHF
Gene expression level
padj = 0.016* Isl1
padj = 2.49E-09* Mef2c
padj = 7.75E-24* Id2
padj = 0.001* Pdfgra
padj = 1.10E-06* Pitx2
padj = 1.79E-09* Mpped2
padj = 1.77E-20* Foxp1
padj = 0.001* Crabp2
padj = 9.03E-19* Tgfbi
padj = 4.37E-17* Irx3
padj = 0.018* Bmpr2
padj = 8.75E-27* Hes1
CNTRL
matHG
DAPI Hand2 GFP
C
D
E
CNTRL
OFT
E9.5
F
G
H
matHG
OFT
E9.5
DAPI Nkx2-5 GFP
I
J
K
CNTRL
OFT
RV
E9.5
L
M
N
matHG
OFT
RV
E9.5
O
Maternal teratogen-induced CHD model
Normal pregnancy
embryonic exposure to CNTRL environment
normal SHF-progenitor cell properties
RV
OFT
LA
RV
LV
Isl1+Tnnt2+ CM
CM differentiation
Normal cardiac development
Maternal PGDM
embryonic exposure to matHG
impaired SHF-cell response
GRN
Isl1
Dose ∞ Severity
RV
OFT
LA
RV
LV
Isl1+Tnnt2+ CM
CM differentiation
PGDM-induced CHD

Figure 7

Fig. 7. Perturbations in the Isl1-gene regulatory network are intrinsic to maternal hyperglycemia-induced congenital heart disease

(A) *Isl1*-dependent gene-regulatory network (GRN) generated by combining String database and experimentally established protein-protein interactions (PPI enrichment p-value < 1.0E-16) show several key mediators of cardiac development. **(B)** Violin plots showing statistically significant gene expression differences between CNTRL vs. matHG-exposed SHF cells at E9.5. All genes represented padj value < 0.05 and were highly significant between the two groups. **(C-N)** Co-immunofluorescent staining of Nkx2-5 or Hand2 (red, shown in insets) with GFP expression driven by Isl1 in E9.5 hearts (n=2) exposed to CNTRL and matHG conditions. The $GFP^{+}Hand2^{+}$ cells in E9.5 outflow tract (OFT) were decreased in matHG-exposed embryos (**E, H;** yellow arrowheads). While fewer $GFP^{+}Nkx2\text{-}5^{+}$ cells (in yellow) were seen in E9.5 OFT and right ventricular (RV)-myocardium with matHG as compared to CRTNL (**J, K, M, N,** yellow arrowheads). Nuclei stained with DAPI are in blue. **(O)** The proposed model describing the underlying cellular and molecular response in embryonic heart exposed to matHG compared to normal cardiovascular development under normal pregnancy (made in ©BioRender). Hyperglycemic dosage is linked to severity of congenital heart disease (CHD) in the offspring. Yellow asterisk indicates ventricular septal defects exhibited in hyperglycemia-exposed embryos. Scale bars: 100μm (C, F) and 20μm (D-H and J-N).

Table 1. Intrauterine exposure to low and higher dosage of maternal hyperglycemia and rate of CHD

Maternal status	Non-STZ-treated (CNTRL)		STZ-treated # (Low-matHG)		STZ-treated # (High-matHG)	
Developmental stage	# of embryos	% heart phenotypes	# of embryos	% heart phenotypes	# of embryos	% heart phenotypes
E9.5-CNTRL	23	0 (0%)	-	-	-	-
E9.5-matHG	-	-	20	3 (15%)	24	6 (25%) *
E11.5-CNTRL	25	0 (0%)	-	-	-	-
E11.5-matHG	-	-	23	5 (21.7%)	23	7 (30.4%) *
E13.5-CNTRL	26	0 (0%)	-	-	-	-
E13.5-matHG	-	-	20	4 (20%)	25	9 (36%) *
E15.5-CNTRL	21	0 (0%)	-	-	-	-
E15.5-matHG	-	-	26	2 (7.7%)	24	4 (16.7%)

#Each embryo may have more than one type of defect.

* indicates differences between three groups to be statistically significant ($p<0.05$).

References

1. E. J. Benjamin *et al.*, Heart Disease and Stroke Statistics-2017 Update: A Report From the American Heart Association. *Circulation* **135**, e146-e603 (2017).
2. J. I. Hoffman, S. Kaplan, The incidence of congenital heart disease. *J Am Coll Cardiol* **39**, 1890-1900 (2002).
3. G. M. Blue, E. P. Kirk, G. F. Sholler, R. P. Harvey, D. S. Winlaw, Congenital heart disease: current knowledge about causes and inheritance. *Med J Aust* **197**, 155-159 (2012).
4. S. Zaidi, M. Brueckner, Genetics and Genomics of Congenital Heart Disease. *Circ Res* **120**, 923-940 (2017).
5. S. N. Nees, W. K. Chung, Genetic Basis of Human Congenital Heart Disease. *Cold Spring Harb Perspect Biol* **12**, (2020).
6. S. N. Nees, W. K. Chung, The genetics of isolated congenital heart disease. *Am J Med Genet C Semin Med Genet* **184**, 97-106 (2020).
7. A. J. Agopian *et al.*, Genome-Wide Association Studies and Meta-Analyses for Congenital Heart Defects. *Circ Cardiovasc Genet* **10**, e001449 (2017).
8. J. J. Schott *et al.*, Congenital heart disease caused by mutations in the transcription factor NKX2-5. *Science* **281**, 108-111 (1998).
9. D. W. Benson *et al.*, Mutations in the cardiac transcription factor NKX2.5 affect diverse cardiac developmental pathways. *J Clin Invest* **104**, 1567-1573 (1999).
10. J. L. M. Moreau *et al.*, Gene-environment interaction impacts on heart development and embryo survival. *Development* **146**, (2019).
11. G. J. Mahler, J. T. Butcher, Cardiac developmental toxicity. *Birth Defects Res C Embryo Today* **93**, 291-297 (2011).
12. R. M. Simeone *et al.*, Diabetes and congenital heart defects: a systematic review, meta-analysis, and modeling project. *Am J Prev Med* **48**, 195-204 (2015).
13. N. Oyen *et al.*, Prepregnancy Diabetes and Offspring Risk of Congenital Heart Disease: A Nationwide Cohort Study. *Circulation* **133**, 2243-2253 (2016).
14. T. T. Hoang, L. K. Marengo, L. E. Mitchell, M. A. Canfield, A. J. Agopian, Original Findings and Updated Meta-Analysis for the Association Between Maternal Diabetes and Risk for Congenital Heart Disease Phenotypes. *Am J Epidemiol* **186**, 118-128 (2017).
15. T. T. Hoang *et al.*, The Congenital Heart Disease Genetic Network Study: Cohort description. *PLoS One* **13**, e0191319 (2018).
16. M. R. Hutson, M. L. Kirby, Model systems for the study of heart development and disease. Cardiac neural crest and conotruncal malformations. *Semin Cell Dev Biol* **18**, 101-110 (2007).
17. M. Basu, V. Garg, Maternal hyperglycemia and fetal cardiac development: Clinical impact and underlying mechanisms. *Birth Defects Res* **110**, 1504-1516 (2018).
18. E. Helle, J. R. Priest, Maternal Obesity and Diabetes Mellitus as Risk Factors for Congenital Heart Disease in the Offspring. *J Am Heart Assoc* **9**, e011541 (2020).
19. S. M. Meilhac, M. E. Buckingham, The deployment of cell lineages that form the mammalian heart. *Nat Rev Cardiol* **15**, 705-724 (2018).
20. E. Nathan *et al.*, The contribution of Islet1-expressing splanchnic mesoderm cells to distinct branchiomeric muscles reveals significant heterogeneity in head muscle development. *Development* **135**, 647-657 (2008).
21. L. A. Dyer, M. L. Kirby, The role of secondary heart field in cardiac development. *Dev Biol* **336**, 137-144 (2009).
22. R. G. Kelly, The second heart field. *Curr Top Dev Biol* **100**, 33-65 (2012).
23. F. Rochais, K. Mesbah, R. G. Kelly, Signaling pathways controlling second heart field development. *Circ Res* **104**, 933-942 (2009).
24. B. L. Black, Transcriptional pathways in second heart field development. *Semin Cell Dev Biol* **18**, 67-76 (2007).
25. C. Kwon *et al.*, A regulatory pathway involving Notch1/beta-catenin/Isl1 determines cardiac progenitor cell fate. *Nat Cell Biol* **11**, 951-957 (2009).
26. M. Basu *et al.*, Epigenetic mechanisms underlying maternal diabetes-associated risk of congenital heart disease. *JCI Insight* **2**, (2017).

27. R. Cerychova *et al.*, Adverse effects of Hif1a mutation and maternal diabetes on the offspring heart. *Cardiovasc Diabetol* **17**, 68 (2018).
28. F. Wang, Y. Wu, M. J. Quon, X. Li, P. Yang, ASK1 mediates the teratogenicity of diabetes in the developing heart by inducing ER stress and inhibiting critical factors essential for cardiac development. *Am J Physiol Endocrinol Metab* **309**, E487-499 (2015).
29. M. Zhao *et al.*, Association of Maternal Diabetes Mellitus and Polymorphisms of the NKX2.5 Gene in Children with Congenital Heart Disease: A Single Centre-Based Case-Control Study. *J Diabetes Res* **2020**, 3854630 (2020).
30. S. D. Kumar, S. T. Dheen, S. S. Tay, Maternal diabetes induces congenital heart defects in mice by altering the expression of genes involved in cardiovascular development. *Cardiovasc Diabetol* **6**, 34 (2007).
31. T. Y. de Soysa *et al.*, Single-cell analysis of cardiogenesis reveals basis for organ-level developmental defects. *Nature* **572**, 120-124 (2019).
32. G. Li *et al.*, Transcriptomic Profiling Maps Anatomically Patterned Subpopulations among Single Embryonic Cardiac Cells. *Dev Cell* **39**, 491-507 (2016).
33. S. C. Morgan, F. Relaix, L. L. Sandell, M. R. Loeken, Oxidative stress during diabetic pregnancy disrupts cardiac neural crest migration and causes outflow tract defects. *Birth Defects Res A Clin Mol Teratol* **82**, 453-463 (2008).
34. S. C. Kolwicz, Jr., S. Purohit, R. Tian, Cardiac metabolism and its interactions with contraction, growth, and survival of cardiomyocytes. *Circ Res* **113**, 603-616 (2013).
35. C. D. Clark *et al.*, Evolutionary conservation of Nkx2.5 autoregulation in the second heart field. *Dev Biol* **374**, 198-209 (2013).
36. C. Misra, S. W. Chang, M. Basu, N. Huang, V. Garg, Disruption of myocardial Gata4 and Tbx5 results in defects in cardiomyocyte proliferation and atrioventricular septation. *Hum Mol Genet* **23**, 5025-5035 (2014).
37. D. J. McCulley, B. L. Black, Transcription factor pathways and congenital heart disease. *Curr Top Dev Biol* **100**, 253-277 (2012).
38. J. W. Vincentz, R. M. Barnes, A. B. Firulli, Hand factors as regulators of cardiac morphogenesis and implications for congenital heart defects. *Birth Defects Res A Clin Mol Teratol* **91**, 485-494 (2011).
39. M. Azhar *et al.*, Transforming growth factor beta in cardiovascular development and function. *Cytokine Growth Factor Rev* **14**, 391-407 (2003).
40. D. M. Cerqueira *et al.*, In utero exposure to maternal diabetes impairs nephron progenitor differentiation. *Am J Physiol Renal Physiol* **317**, F1318-F1330 (2019).
41. N. Yaras *et al.*, Effects of diabetes on ryanodine receptor Ca release channel (RyR2) and Ca2+ homeostasis in rat heart. *Diabetes* **54**, 3082-3088 (2005).
42. T. Arimura *et al.*, Cardiac ankyrin repeat protein gene (ANKRD1) mutations in hypertrophic cardiomyopathy. *J Am Coll Cardiol* **54**, 334-342 (2009).
43. D. S. Herman *et al.*, Truncations of titin causing dilated cardiomyopathy. *N Engl J Med* **366**, 619-628 (2012).
44. S. Zhuang *et al.*, Expression of Isl1 during mouse development. *Gene Expr Patterns* **13**, 407-412 (2013).
45. Y. Sun *et al.*, Islet 1 is expressed in distinct cardiovascular lineages, including pacemaker and coronary vascular cells. *Dev Biol* **304**, 286-296 (2007).
46. M. Gunthel, P. Barnett, V. M. Christoffels, Development, Proliferation, and Growth of the Mammalian Heart. *Mol Ther* **26**, 1599-1609 (2018).
47. I. Tirosh *et al.*, Dissecting the multicellular ecosystem of metastatic melanoma by single-cell RNA-seq. *Science* **352**, 189-196 (2016).
48. T. Tsuchihashi *et al.*, Hand2 function in second heart field progenitors is essential for cardiogenesis. *Dev Biol* **351**, 62-69 (2011).
49. O. W. Prall *et al.*, An Nkx2-5/Bmp2/Smad1 negative feedback loop controls heart progenitor specification and proliferation. *Cell* **128**, 947-959 (2007).
50. M. Pashmforoush *et al.*, Nkx2-5 pathways and congenital heart disease; loss of ventricular myocyte lineage specification leads to progressive cardiomyopathy and complete heart block. *Cell* **117**, 373-386 (2004).
51. T. Araki *et al.*, Mouse model of Noonan syndrome reveals cell type- and gene dosage-dependent effects of Ptpn11 mutation. *Nat Med* **10**, 849-857 (2004).
52. M. Maitra *et al.*, Interaction of Gata4 and Gata6 with Tbx5 is critical for normal cardiac development. *Dev Biol* **326**, 368-377 (2009).

53. I. S. Kathiriya *et al.*, Modeling Human TBX5 Haploinsufficiency Predicts Regulatory Networks for Congenital Heart Disease. *Dev Cell* **56**, 292-309 e299 (2021).
54. Y. S. Ang *et al.*, Disease Model of GATA4 Mutation Reveals Transcription Factor Cooperativity in Human Cardiogenesis. *Cell* **167**, 1734-1749 e1722 (2016).
55. C. V. Theodoris *et al.*, Human disease modeling reveals integrated transcriptional and epigenetic mechanisms of NOTCH1 haploinsufficiency. *Cell* **160**, 1072-1086 (2015).
56. M. Hachisuga *et al.*, Hyperglycemia impairs left-right axis formation and thereby disturbs heart morphogenesis in mouse embryos. *Proc Natl Acad Sci U S A* **112**, E5300-5307 (2015).
57. D. E. Scott-Drechsel, S. Rugonyi, D. L. Marks, K. L. Thornburg, M. T. Hinds, Hyperglycemia slows embryonic growth and suppresses cell cycle via cyclin D1 and p21. *Diabetes* **62**, 234-242 (2013).
58. M. S. Winzell, B. Ahren, The high-fat diet-fed mouse: a model for studying mechanisms and treatment of impaired glucose tolerance and type 2 diabetes. *Diabetes* **53 Suppl 3**, S215-219 (2004).
59. C. A. Loffredo, P. D. Wilson, C. Ferencz, Maternal diabetes: an independent risk factor for major cardiovascular malformations with increased mortality of affected infants. *Teratology* **64**, 98-106 (2001).
60. J. Cao *et al.*, A human cell atlas of fetal gene expression. *Science* **370**, (2020).
61. M. Asp *et al.*, A Spatiotemporal Organ-Wide Gene Expression and Cell Atlas of the Developing Human Heart. *Cell* **179**, 1647-1660 e1619 (2019).
62. C. Tabula Muris *et al.*, Single-cell transcriptomics of 20 mouse organs creates a Tabula Muris. *Nature* **562**, 367-372 (2018).
63. D. M. DeLaughter *et al.*, Single-Cell Resolution of Temporal Gene Expression during Heart Development. *Dev Cell* **39**, 480-490 (2016).
64. A. Moretti, J. Lam, S. M. Evans, K. L. Laugwitz, Biology of Isl1+ cardiac progenitor cells in development and disease. *Cell Mol Life Sci* **64**, 674-682 (2007).
65. L. Ma *et al.*, ISL1 loss-of-function mutation contributes to congenital heart defects. *Heart Vessels* **34**, 658-668 (2019).
66. H. Zhang *et al.*, The LIM-homeodomain protein ISL1 activates insulin gene promoter directly through synergy with BETA2. *J Mol Biol* **392**, 566-577 (2009).
67. P. Quijada, M. A. Trembley, E. M. Small, The Role of the Epicardium During Heart Development and Repair. *Circ Res* **126**, 377-394 (2020).
68. R. Soldatov *et al.*, Spatiotemporal structure of cell fate decisions in murine neural crest. *Science* **364**, (2019).
69. A. Butler, P. Hoffman, P. Smibert, E. Papalexi, R. Satija, Integrating single-cell transcriptomic data across different conditions, technologies, and species. *Nat Biotechnol* **36**, 411-420 (2018).
70. E. Becht *et al.*, Dimensionality reduction for visualizing single-cell data using UMAP. *Nat Biotechnol*, (2018).
71. M. I. Love, W. Huber, S. Anders, Moderated estimation of fold change and dispersion for RNA-seq data with DESeq2. *Genome Biol* **15**, 550 (2014).
72. C. Ziegenhain *et al.*, Comparative Analysis of Single-Cell RNA Sequencing Methods. *Mol Cell* **65**, 631-643 e634 (2017).
73. X. Qiu *et al.*, Reversed graph embedding resolves complex single-cell trajectories. *Nat Methods* **14**, 979-982 (2017).
74. K. Street *et al.*, Slingshot: cell lineage and pseudotime inference for single-cell transcriptomics. *BMC Genomics* **19**, 477 (2018).

Acknowledgments:

The authors thank members of the Biomorphology core for histology support and The Steve and Cindy Rasmussen Institute for Genomic Medicine at Nationwide Children's Hospital for preliminary sequencing analysis. The authors are grateful to Kedryn K Baskin for helpful comments and critical review of the manuscript. **Funding**: This work was supported by funding from the American Heart Association and the Children Heart Foundation Career Development Award Grant 18CDA34110330 (M.B), National Institute of Health grants: R01 HL144009 (V.G.), NHLBI Postdoctoral Fellowship T32 HL098039 (S.M). **Author contributions**: MB conceived the project, designed, supervised the experiments with input from VG. MB performed immunohistochemical characterization, generated single-cell libraries, acquired all the data and analyzed the experiments. VG offered substantial intellectual contribution throughout the project and revised the manuscript. SM performed bioinformatics analysis of scRNA-seq data, pseudotime trajectory analysis using Monocle and Slingshot and developed the Seurat-based graphical user interface. The murine studies were performed by CM and MB. CM performed STZ injections, embryo collection, genotyping, sectioning and histological imaging and quantification. XZ performed initial scRNA-seq data processing. MK generated control E11.5 single-cell library. UM performed quantification of E15.5 embryos. SM and MB interpreted the scRNA-seq data with input from VG. MB, SM and CM wrote and edited the manuscript with input from all the authors.

Competing interests: Authors declare no competing interests.

Data and materials availability: The authors declare that all supporting data are available within the article and its Supplemental Materials. The scRNA sequencing data is available at the NCBI GEO accession number. The mouse models are commercially available from Jackson Laboratory, USA. Any other relevant data are available from the lead corresponding author upon reasonable request. Source data are provided with this paper.

Supplementary Materials for

Maternal hyperglycemia impedes second heart field-derived cardiomyocyte differentiation to elevate the risk of congenital heart defects

Sathiyanarayanan Manivannan[1,2#], Corrin Mansfield[1,2#], Xinmin Zhang[3], Karthik. M. Kodigepalli[4], Uddalak Majumdar[1,2], Vidu Garg[1,2,5,6*] and Madhumita Basu[1,2,5*]

This PDF file includes:

Supplemental Materials and Methods

Supplemental Figures. S1 to S9

Supplemental Figure legends of S1 to S9

Supplemental Tables S1 to S11

Supplemental Materials and Methods

Generation of chemically-induced maternal pre-gestational diabetes mellitus (PGDM) murine model

Wildtype (*wt*) C57BL/6J mice were purchased from Jackson Laboratory (Stock Nos: 000664) for this study. A subset of six- to eight-week-old female mice (~15-18g body weight) were used to chemically induce type 1-like DM. Mice fasted for an hour before treatment and Streptozotocin (STZ, Fisher Scientific; NC0146241), dissolved in 0.01 mol/l citrate buffer (pH 4.5) was intraperitoneally injected at 75 mg/kg/bodyweight for 3 consecutive days, as previously published (*26*). Seven days post-STZ treatment, mice fasted for ~8 hours during the light cycle, and blood glucose (B.G.) levels were checked using the AlphaTrak veterinary blood glucometer calibrated specifically for rodents from tail vein blood (Abbott Laboratories). Blood glucose was documented before initiating the timed breeding and during embryo collection. Mice with fasting blood glucose ≥200 mg/dl (11 mmol/l) were defined as HG following previously published protocol. If the mice did not achieve the threshold after 7 days, blood glucose levels were re-tested after fourteen days of STZ injection.

Dissection of mouse embryos exposed to maternal control and hyperglycemic environment

STZ-treated (matHG) and non-STZ-treated (CNTRL) females were timed bred overnight with *wt* C57BL/6J males. Mice were maintained on a 12-hour-light/dark cycle, and in the

morning, when a vaginal plug was observed it indicated embryonic day (E) 0.5. Pregnant mothers were monitored regularly and sacrificed for embryo harvest at E9.5, E11.5, E13.5 and E15.5. Based on the interquartile distribution of maternal B.G. levels, the STZ-treated females were further stratified into two categories: (i) low-matHG and (ii) high-matHG groups. All the mice were housed at the animal facility per Nationwide Children's Hospital, Abigail Wexner Research Institute's Animal Resource Center policies, and the NIH's *Guide for the Care and Use of Laboratory Animals* (National Academies Press, 2011). All animal research has been reviewed and approved by an Institutional Animal Care and Use Committee (protocol #s AR13-00056 and AR20-00029).

Histological characterization of embryonic hearts

Embryos at E9.5, E11.5, E13.5 and E15.5 stages were collected from CNTRL, low and high-matHG groups for histological analysis. Embryos were harvested, fixed in 10% formalin (Fisher Scientific; SF98-4) overnight and changed to 1X PBS after 24hrs of fixation. Tissues were processed overnight in ethanol and paraffin embedded at the Morphology Core in Nationwide Children's Hospital (NCH). To visualize morphological characteristics, 7µm thick transverse sections were stained with Hematoxylin & Eosin (Sigma) following the manufacturer's protocol and imaged using Zeiss AxioImagerA2.

Dissection of mouse embryonic hearts and workflow of single-cell RNA-sequencing

To prepare scRNA-seq, the entire cardiogenic region was micro-dissected from E9.5 and E11.5 embryos harvested from *wt* STZ-treated high-matHG and untreated CNTRL female mice. Maternal B.G. levels were tested just before harvesting embryos to ensure diabetic status in CNTRL and STZ-treated females. First, embryos were removed from the yolk-sac, dissected in diethylpyrocarbonate-treated 1X ice-cold PBS and placed in 1XPBS. Dissected cardiac tissue was incubated in 1mg/ml Collagenase II (Worthington; LS004176) and 1X TrypLE™ Select Enzyme (ThermoFisher Scientific, #12563029) for 15 mins (for E9.5) and 25 mins (for E11.5) at 37°C dry bath with occasional stirring every 5 mins for complete dissociation. The Collagenase/TrypLE solution was quenched immediately with complete DMEM media supplemented with 10% FBS and pelleted down at 1000 rpm for 5 mins at 4°C. Cell pellets were dissolved in 0.04% bovine serum albumin, BSA (Fisher Scientific, #BP9703100) made in PBS and filtered through a 40µm cell strainer (BD Falcon, #352340), centrifuged at 1000 rpm for 5 mins at 4°C, and resuspended in 50µl 0.04% BSA/PBS. Cell viabilities (>85-92%) were assessed using the Trypan blue (1450013; Bio-Rad) exclusion method on Countess™ II FL Automated Cell Counter (ThermoFisher; AMQAF1000). Single-cell libraries targeting ~4000 cell recovery/sample were generated using 10X Genomics Chromium controller according to the manufacturer's instructions using Chromium Single Cell 3′ Reagent Kit (v2 chemistry; PN-120237). The cDNA and libraries were generated using the Chromium Single Cell 3′ Library & Gel Bead Kit v2 and Chromium i7 Multiplex Kit (10X, PN-120237, PN-120262) following the manufacturer's suggested protocol. The quality and concentrations of cDNA from each sample were measured using High Sensitivity D5000 ScreenTape® on Agilent

2200 TapeStation. After adjusting all four samples (CNTRL vs. matHG-exposed E9.5 and E11.5) to similar concentrations, each single-cell cDNA sample was used for library preparation and quantified using High Sensitivity D1000 ScreenTape®. Single-cell libraries were sequenced on the Illumina Hiseq4000 platform with 2 X 150 bp read length at the Institute for Genomic Medicine in NCH. CNTRL and matHG-exposed E9.5 libraries were pooled and sequenced in the same lane. Similarly, CNTRL and matHG-exposed E11.5 single-cell libraries were pooled together and sequenced in the same lane. Sequencing parameters were selected according to the Chromium Single Cell v2 specifications. All libraries were sequenced to a mean read depth of at least 50,000 reads per cell.

Single-cell RNA-seq data pre-processing, quality control and unsupervised clustering:

We used cellranger pipeline to demultiplex and convert Illumina bcl output into fastq files. We mapped the fastq reads to the mouse genome mm10 (GRCm38.p6) and gene annotation downloaded from NCBI (https://www.ncbi.nlm.nih.gov/assembly/GCF_000001635.26). Using the cellranger count function we generated count matrix output for each gene within each cell. A violin plot for each object was created to visualize the distribution of reads captured and the quality of total capture. Cells of low quality or those representing doublets were excluded from our analyses. After implementing the cutoff for number of genes expressed (*nFeature_RNA* function) set to 500-7000 and < 10% percentage of mitochondrial gene

expression relative to total expression of the cell (*percent.mt* function), we obtained 2823, 3239, 3836 and 3229 cells from CNTRL-E9.5, CNTRL-E11.5, matHG-E9.5 and matHG-E11.5 respectively. This data was processed using Seurat version 3.0 R package to perform normalization and identify genes with the highest variability (*69*). The data was scaled and dimensionality reduction was performed using Seurat and clustering of cells was visualized in two dimensions using Uniform Manifold Approximation and Projection (UMAP)(*70*). Briefly, we added 'DevStage' and 'Maternal' meta information to each Seurat object to define the developmental stage and the diabetes state of the dam, respectively. Next, we combined the data using regularized negative binomial regression ('sctransform' function in Seurat) and canonical correlation analysis (CCA) based integration. We also tried integration without 'sctransform' function and using 50 dimensions to obtain a merged dataset. There was no significant difference in the clustering of cells based on the two approaches. We performed dimensionality reduction and clustering of cells on the integrated data using a very broad clustering parameter (resolution = 0.2).

Cell type identification and sub-clustering analysis:

After removing the low-quality and non-mesodermal cells (ectoderm, endoderm-derived and blood cells) from each sample, filtering and unsupervised cell-clustering analyses were performed with the Seurat v3 R package, as described earlier. Marker genes were identified for individual clusters using a minimum percent expression of 50% and log_2fold change threshold of 0.25 (log_2FC.threshold). From each cluster, the top 5 markers were selected based on average log_2FC and used to classify each cluster. The clusters were

also cross-referenced with known cell-type specific marker gene expression using publicly available wildtype scRNA-seq datasets at other embryonic time points (*31, 32*). Similarly, all reclustering analyses (on multipotent progenitor cell and cardiomyocyte subpopulations) were processed as described above.

Differential gene expression analysis:

Cluster-specific differential gene expression analysis was performed between embryonic developmental stage and maternal diabetic status. Within each group, we combined counts obtained for each gene to produce three in silico replicates of gene vs. expression count matrix. These in silico replicates were then analyzed using DESeq2 to identify differentially expressed genes between various conditions (*71*). Owing to the high drop-out rate observed in the 10X Drop-seq method, our approach to combine counts reduces noise and brings the data closer to bulk-RNA seq data which are conventionally used in the DESeq2 pipeline (*71, 72*).

Pseudo-time trajectory analysis:

Cell trajectory analyses were performed on matHG-exposed E9.5 and E11.5 vs. CNTRL E9.5 and E11.5 multipotent progenitor cell and cardiomyocytes subpopulations using the Monocle 2 (http://cole-trapnell-lab.github.io/monocle-release/) and Slingshot version 1.8.0 packages (*73, 74*). Differentially expressed genes were determined using the *FindAllMarkers* function in Seurat v3 package for temporal ordering of these cardiac cells along the differentiation trajectory in response to CNTRL vs. maternal HG environment.

Second heart field cell-lineage tracing in response to maternal hyperglycemic exposure in utero:

For *Isl-1*-derived cardiac cell-lineage tracing studies, we purchased *Isl-1Cre*$^{+/-}$ male mice and *Rosa*$^{mT/mG}$ reporter mice from Jackson Laboratory (Stock Nos: 024242 and 007676). Adult males were bred with STZ-treated and untreated homozygous *Rosa*$^{mT/mG}$ female mice. Type 1 diabetes mellitus (T1DM) was induced in females as described earlier and B.G. levels were tested 7-14 days post-STZ treatment. Following successful breeding CNTRL and matHG-exposed *Isl-1Cre*$^{+}$*; Rosa*$^{mTmG/+}$ embryos at E9.5, E11.5, and E13.5 were harvested and compared with *Cre*$^{-}$ littermate controls. Embryos were fixed at 4% paraformaldehyde for 24 hours and changed to PBS. TdTomato and GFP fluorescence intensities of whole embryos were captured using an Olympus BX51 microscope.

Immunofluorescence staining:

For immunofluorescence (IF) staining, E9.5, E11.5, E13.5 formalin-fixed paraffin-embedded cardiac sections were deparaffinized using xylene and grades of ethanol, followed by antigen retrieval using citrate-based Antigen Unmasking solution (H-3300, Vector laboratories) using standard protocols (*26*). After permeabilization and blocking with 1% BSA in PBS-Triton X-100 for 1 hour, tissue sections were probed overnight at 4°C with primary antibodies including rat α-Endomucin (1:250; Millipore; MAB2624); rabbit α-Phospho-Histone H3 (1:250; EMD Millipore; 06-570), mouse α-Cardiac Troponin T (1:250; Abcam; ab8295), rabbit α-Periostin (1:250; Abcam; ab14041), rabbit α-

Transgelin (1:250; Abcam; ab14106), rabbit α-Fibronectin (1:250; Abcam; ab2413), and rabbit α-GFP (1:250; ab290; Abcam). Following series of washing, sections were incubated with donkey α-rat, α-rabbit, and α-mouse secondary antibodies conjugated to Alexa Fluor 594/488 for 1 hour at room temperature in the dark. After washing, sections were counterstained with Vectashield HardSet Antifade Mounting Medium with DAPI (Vector laboratories). The images were visualized using Olympus BX51 and Zeiss AxioImagerA2. All staining experiments were performed at least in triplicate.

Statistical analysis

All experiments were performed at least in triplicate and data represented as mean ± SEM unless otherwise mentioned. Two-tailed Student's *t*-test, One-way ANOVA with Bonferroni's multiple comparisons test and 2X2 and 3X2 chi-square test with Yate's correction (for categorical data) were performed to determine statistical significance using GraphPad Prism 8 software package. *, $p \leq 0.05$ considered to be statistically significant.

Supplemental figures and figure legends.

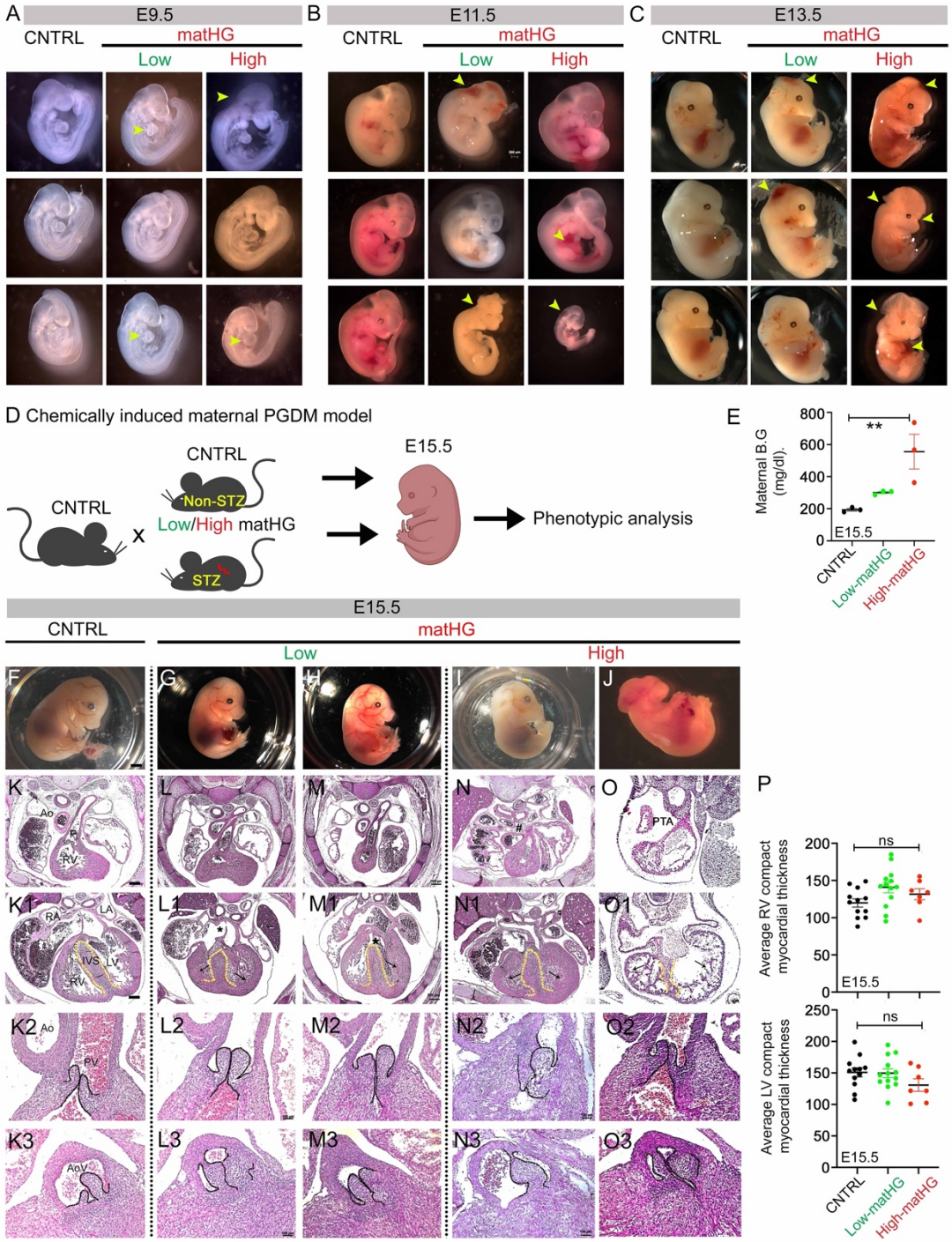

Figure S1

Fig. S1. Phenotypic characterization of embryos exposed to matHG dosage

(A-C) Whole embryo images of E9.5, E11.5, and E13.5 embryos from control (CNTRL), low and high-maternal hyperglycemia (matHG)-environment. A spectrum of defects including cardio-craniofacial malformations, exencephaly, pericardial effusion, chest and brain hemorrhage, and reduced body size were noted in the embryos of diabetic mother (yellow arrowheads). **(D)** Diagram represents wildtype CNTRL and streptozotocin (STZ)-treated matHG females bred with NG males and E15.5 embryos were examined for morphological analysis, made in ©BioRender. **(E)** Distribution of maternal blood glucose (B.G.) levels in CNTRL vs. low and high-matHG groups during the embryo harvest showed significant elevation in hyperglycemia. **(F-J)** Gross morphological features were shown in the E15.5 embryos exposed to CNTRL and low vs. high-matHG dams. **(K-O)** Histological images demonstrate ventricular hypertrophy (black arrows), mild ventricular septal defects (indicated by *), increasing trend towards septal thickening (yellow dotted lines), semilunar valve thickening (black dotted lines) to persistent truncus arteriosus (PTA) in E15.5 embryos subjected to low-to-high matHG exposure compared to CNTRL embryos. **(P)** Average right and left ventricular (RV and LV) wall thickness was quantified between experimental and CNTRL embryos. Data presented as mean $\pm$ SEM. ns=non-significant; ** indicates significant p-value after one-way ANOVA analysis with Bonferroni correction using GraphPad Prism 8. Scale bars: A= 200µm; B, C, F-J = 500µm, K-O: 200 and 100µm).

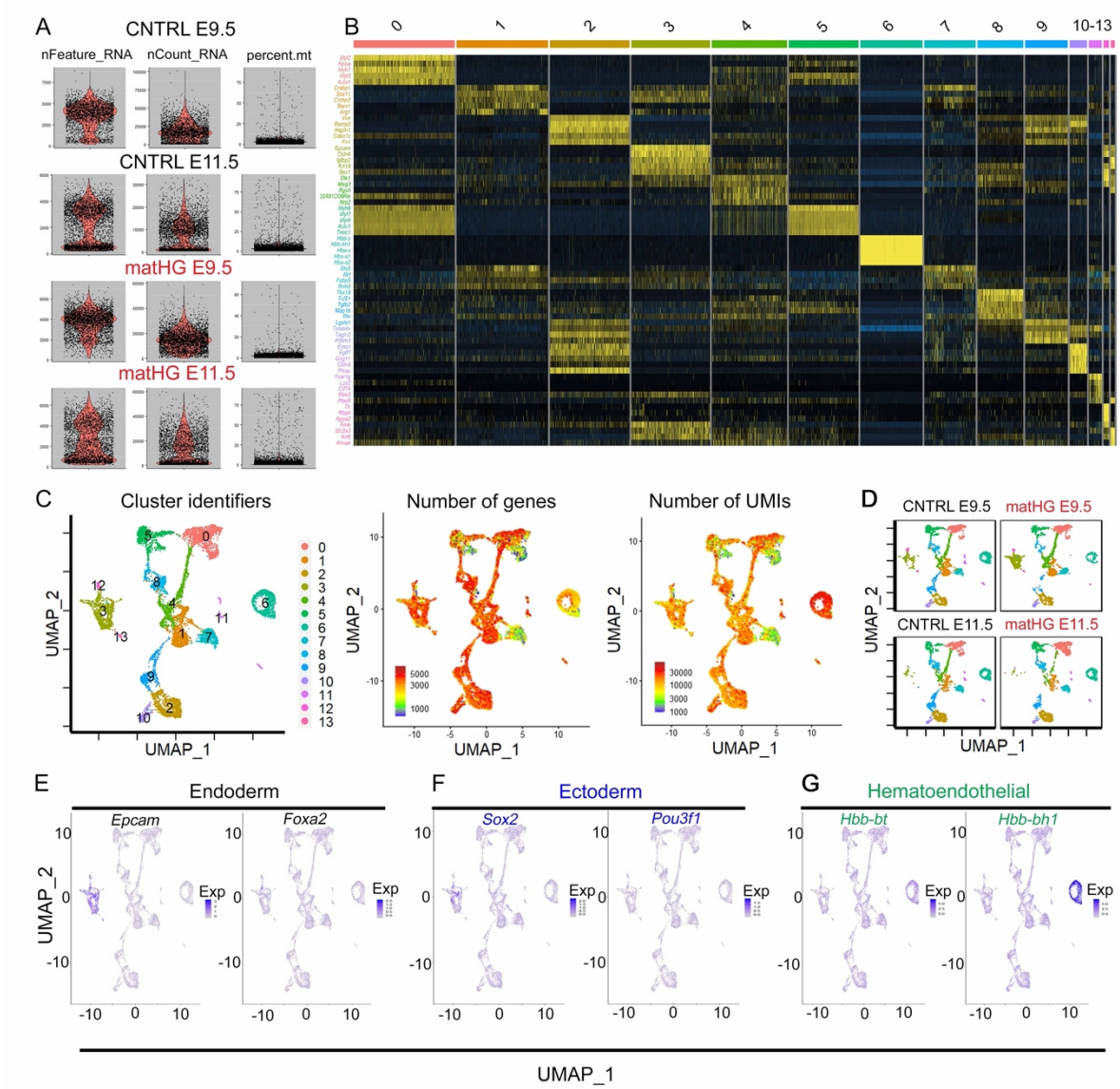

Figure S2

Fig. S2. Quality control and normalization of *in vivo* single-cell transcriptomics data

(A) Quality control of scRNA-seq data obtained from E9.5 and E11.5 hearts exposed to control (CNTRL) and hyperglycemia (matHG) environment. From each sample, cells presenting a cutoff nFeature_RNA set to 500-7000 and <10% mitochondrial content only chosen for further analysis. **(B)** Unsupervised clustering revealed a total of 14 clusters (0-13) and the top five genes per cluster are indicated in the heatmap. **(C, D)** Uniform

manifold approximation and projection (UMAP) plots show all captured clusters colored by their identities, number of genes and number of unique molecular identifiers (UMIs) in merged and split E9.5 and E11.5 scRNA-seq datasets. **(E-G)** UMAP plots show the non-mesodermal clusters with highest expression of *Epcam*, *Foxa2*, *Sox2*, *Pou3f1*, *Hbb-bt* and *Hbb-bh1*, genes that mark endoderm, ectoderm and hematoendothelial cells and were discarded from subsequent analysis**.**

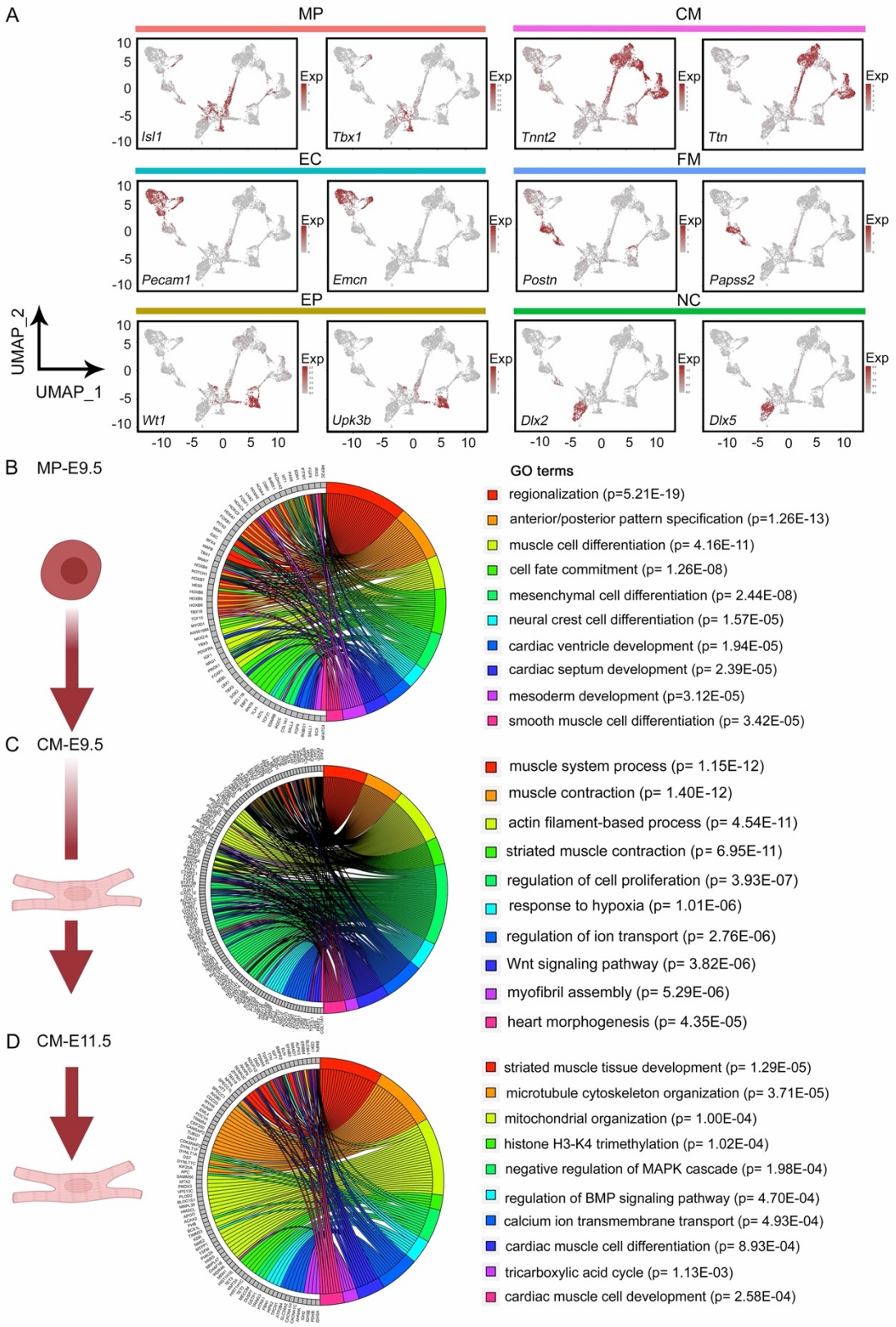
A
MP
CM
EC
FM
EP
NC
Isl1
Tbx1
Tnnt2
Ttn
Pecam1
Emcn
Postn
Papss2
Wt1
Upk3b
Dlx2
Dlx5
Exp
UMAP_2
UMAP_1
B MP-E9.5
C CM-E9.5
D CM-E11.5
GO terms
regionalization (p=5.21E-19)
anterior/posterior pattern specification (p=1.26E-13)
muscle cell differentiation (p= 4.16E-11)
cell fate commitment (p= 1.26E-08)
mesenchymal cell differentiation (p= 2.44E-08)
neural crest cell differentiation (p= 1.57E-05)
cardiac ventricle development (p= 1.94E-05)
cardiac septum development (p= 2.39E-05)
mesoderm development (p=3.12E-05)
smooth muscle cell differentiation (p= 3.42E-05)
muscle system process (p= 1.15E-12)
muscle contraction (p= 1.40E-12)
actin filament-based process (p= 4.54E-11)
striated muscle contraction (p= 6.95E-11)
regulation of cell proliferation (p= 3.93E-07)
response to hypoxia (p= 1.01E-06)
regulation of ion transport (p= 2.76E-06)
Wnt signaling pathway (p= 3.82E-06)
myofibril assembly (p= 5.29E-06)
heart morphogenesis (p= 4.35E-05)
striated muscle tissue development (p= 1.29E-05)
microtubule cytoskeleton organization (p= 3.71E-05)
mitochondrial organization (p= 1.00E-04)
histone H3-K4 trimethylation (p= 1.02E-04)
negative regulation of MAPK cascade (p= 1.98E-04)
regulation of BMP signaling pathway (p= 4.70E-04)
calcium ion transmembrane transport (p= 4.93E-04)
cardiac muscle cell differentiation (p= 8.93E-04)
tricarboxylic acid cycle (p= 1.13E-03)
cardiac muscle cell development (p= 2.58E-04)

Figure S3

Fig. S3. Gene ontology and pathway enrichment analysis of multipotent progenitor and cardiomyocyte clusters with maternal hyperglycemic exposure

(A) Feature plots signify the merged UMAP distribution and demonstrate cluster-specific expression of marker genes (red) applied to classify the cardiac subpopulations. The scale indicates Z-scored expression values. MP = multipotent progenitor, CM=cardiomyocytes, EC= endocardial/endothelial, FM= fibro-mesenchymal, EP= epicardial and NC= neural crest cells. **(B-D)** Gene Ontology (GO) analysis of differentially expressed genes or DEGs (log_2fold change (FC) > 1 or < -1 and $p_{adj} < 0.05$) between CNTRL vs. maternal hyperglycemia (matHG)-exposed E9.5 MP cells were performed. **(B)** E9.5 DEGs were associated with regionalization, differentiation and cell-fate commitment, as shown in the chord plot. **(C, D)** Chord plots representing GO-terms in E9.5 and E11.5 CM show genes associated with cardiac muscle contraction, response to hypoxia, mitochondrial dysfunction, and regulation of Wnt, MAPK and BMP signaling pathways are significantly perturbed under maternal diabetic milieu. The p-values (in parenthesis) indicate statistically significant enrichment for each GO term associated with the clusters. Cell images are made in ©BioRender.

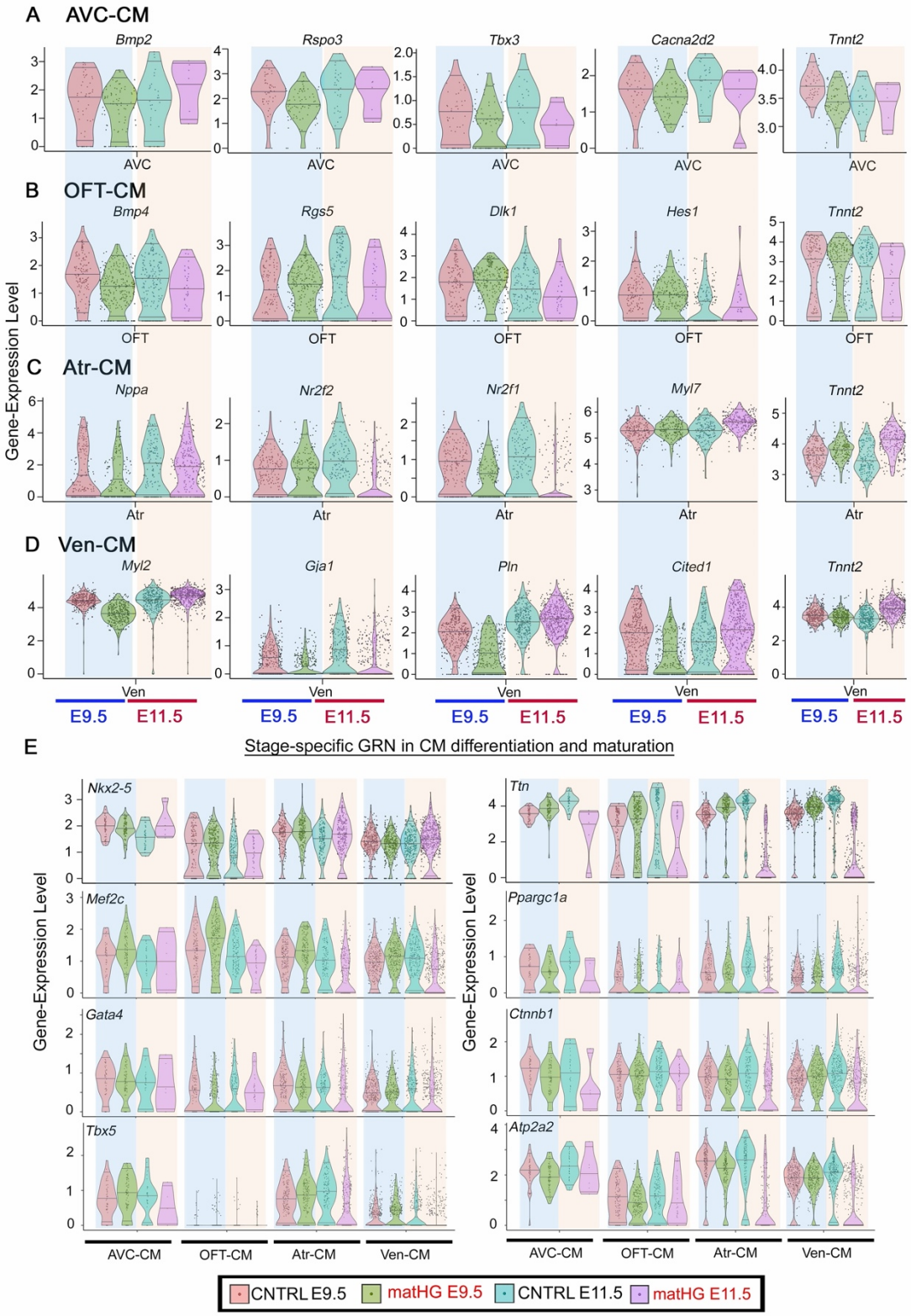
A AVC-CM
Bmp2
Rspo3
Tbx3
Cacna2d2
Tnnt2
AVC
B OFT-CM
Bmp4
Rgs5
Dlk1
Hes1
Tnnt2
OFT
C Atr-CM
Nppa
Nr2f2
Nr2f1
Myl7
Tnnt2
Atr
D Ven-CM
Myl2
Gja1
Pln
Cited1
Tnnt2
Ven
E9.5
E11.5
Gene-Expression Level
E
Stage-specific GRN in CM differentiation and maturation
Nkx2-5
Mef2c
Gata4
Tbx5
Ttn
Ppargc1a
Ctnnb1
Atp2a2
AVC-CM
OFT-CM
Atr-CM
Ven-CM
CNTRL E9.5
matHG E9.5
CNTRL E11.5
matHG E11.5

Figure S4

Fig. S4. Maternal hyperglycemia causes transcriptional dysregulation in cardiomyocyte subpopulations

(A-D) Violin plots show normalized expression levels of genes in cardiomyocyte (CM) subclusters derived from E9.5 and E11.5 hearts subjected to control (CNTRL) and maternal hyperglycemia (matHG). The mRNA expression of *Bmp2*, *Rspo3*, *Tbx3*, *Cacna2d2* in atrioventricular canal (AVC)-CM, *Bmp4*, *Rgs5*, *Dlk1*, *Hes1* in outflow tract (OFT)-CM, *Nppa*, *Nr2f2*, *Nr2f1*, *Myl7* in atrial (Atr)-CM and *Myl2*, *Gja1*, *Pln*, *Cited1* expression in ventricular (Ven)-CM demonstrate a developmental stage-specific response to matHG. Gene expression of common cardiac muscle maker, *Tnnt2* also reveals cluster-specific response to high-matHG exposure. **(E)** Gene regulatory network (GRN), in which genes essential for CM differentiation and maturation were measured using scRNA-seq dataset. Violin plots show developmental stage and maternal diabetic status-specific variabilities in *Nkx2.5, Mef2c, Gata4* and *Tbx5* (cardiac transcription factors) and *Ttn, Ppargc1a, Ctnnb1* and *Atp2a2* (CM maturation markers) in E9.5 and E11.5 myocardial subpopulations.

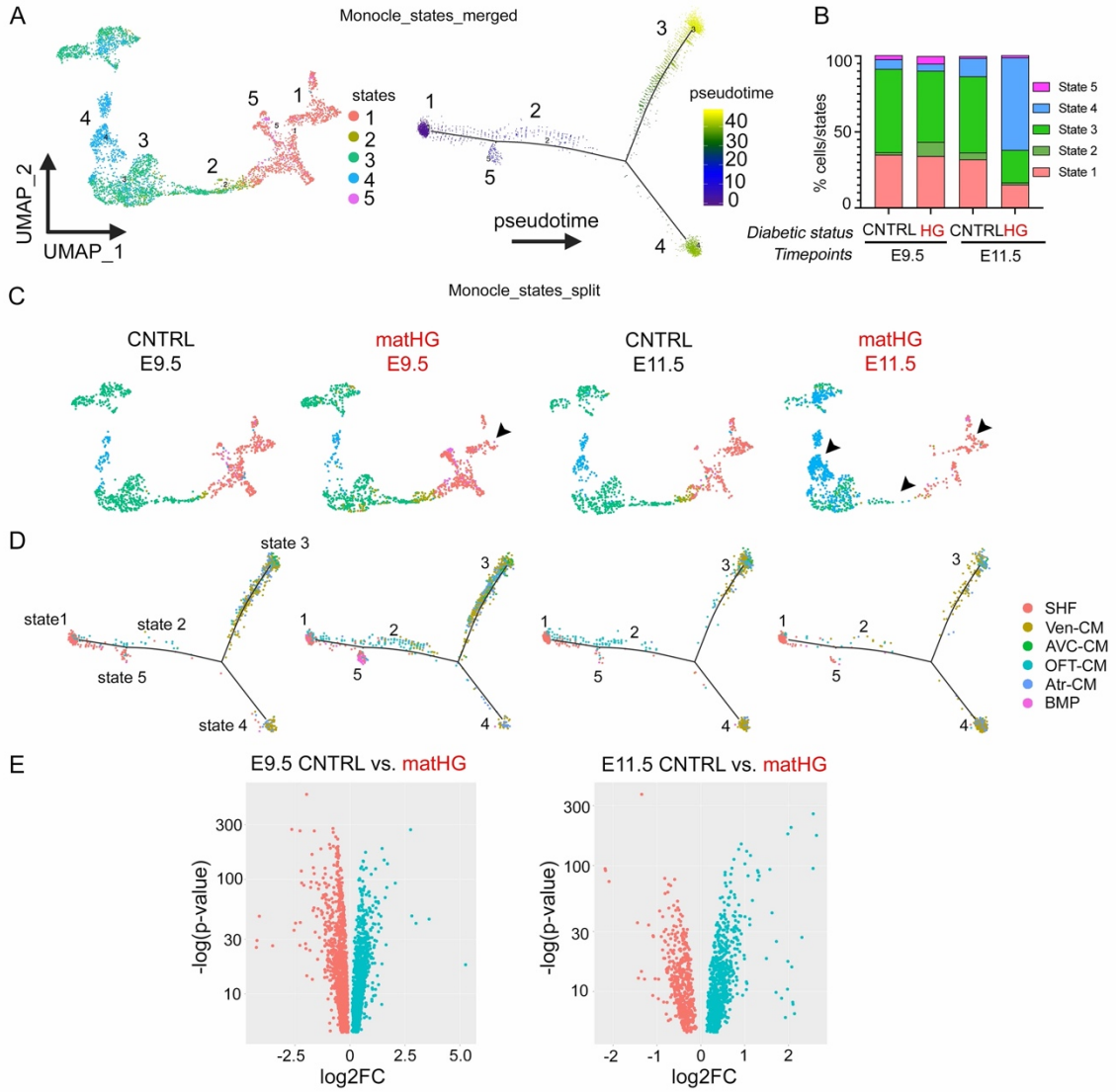

Figure S5

Fig. S5. Transcriptomic changes in MP-CM clusters across pseudotime

(A) Merged UMAP plot of multipotent progenitor (MP) and cardiomyocytes (CM) after subclustering and monocle analysis. Five resultant states (1-5) from combining control (CNTRL) and maternal hyperglycemia (matHG)-exposed E9.5 and E11.5 reveal distribution of cells through pseudotime. (B) Proportion of MP-CM subpopulations per

pseudotime states were plotted as percentages for all four samples. (C, D) Split UMAP and pseudotime plots represent changes between CNTRL and matHG-exposed E9.5 and E11.5. Cardiac subpopulations were superimposed in pseudotime (E) Volcano plots (-log(p-value) in y-axis and log2foldchange in x-axis) show differential gene expression analysis between states and significant changes were noticed among experimental groups at E9.5 and E11.5.

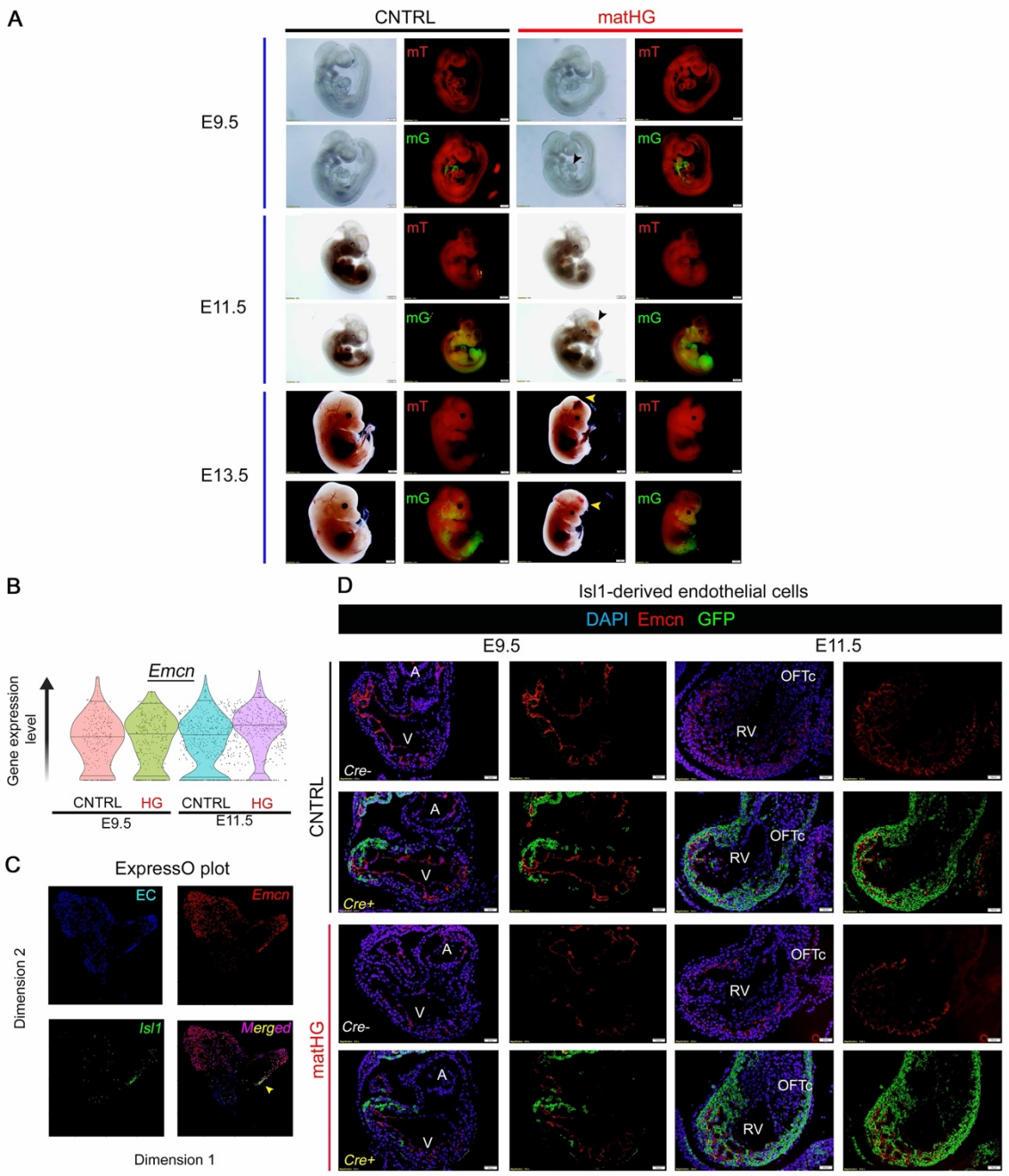

Figure S6

Fig. S6. *Isl1*-cell fate mapping in presence of maternal hyperglycemic exposure

(A) Whole-mount brightfield and fluorescence images of representative *Isl1Cre*$^{+}$; *Rosa*$^{mTmG/+}$ (mG; GFP^{+}) and *Isl1Cre*$^{-}$; *Rosa*$^{mTmG/+}$(mT; GFP^{-}) littermate control hearts at

E9.5, E11.5 and E13.5, exposed to control (CNTRL) and maternal hyperglycemia (matHG) environment. Black and yellow arrowheads indicate hemorrhage and neural tube defects in embryos subjected to matHG in utero. **(B)** Violin plots show no significant change in *Emcn* expression (endothelial cell marker) in E9.5 and E11.5 scRNA-seq data and **(C)** Expresso plot confirmed the presence of very few *Isl1*$^{+}$*Emcn*$^{+}$ cells in endothelial cell (EC) cluster (yellow arrowheads). **(D)** Co-immunostainings show reduced Emcn (red) protein expression in EC with matHG (in both Cre- and Cre+ littermate controls) but no changes in *Isl1*-derived Emcn^{+}GFP^{+} ECs (i-EC, in yellow) were noticed in E9.5 and E11.5 hearts exposed to high-matHG vs. CNTRL. Scale bars: 200µm (A) and 50µm (D).

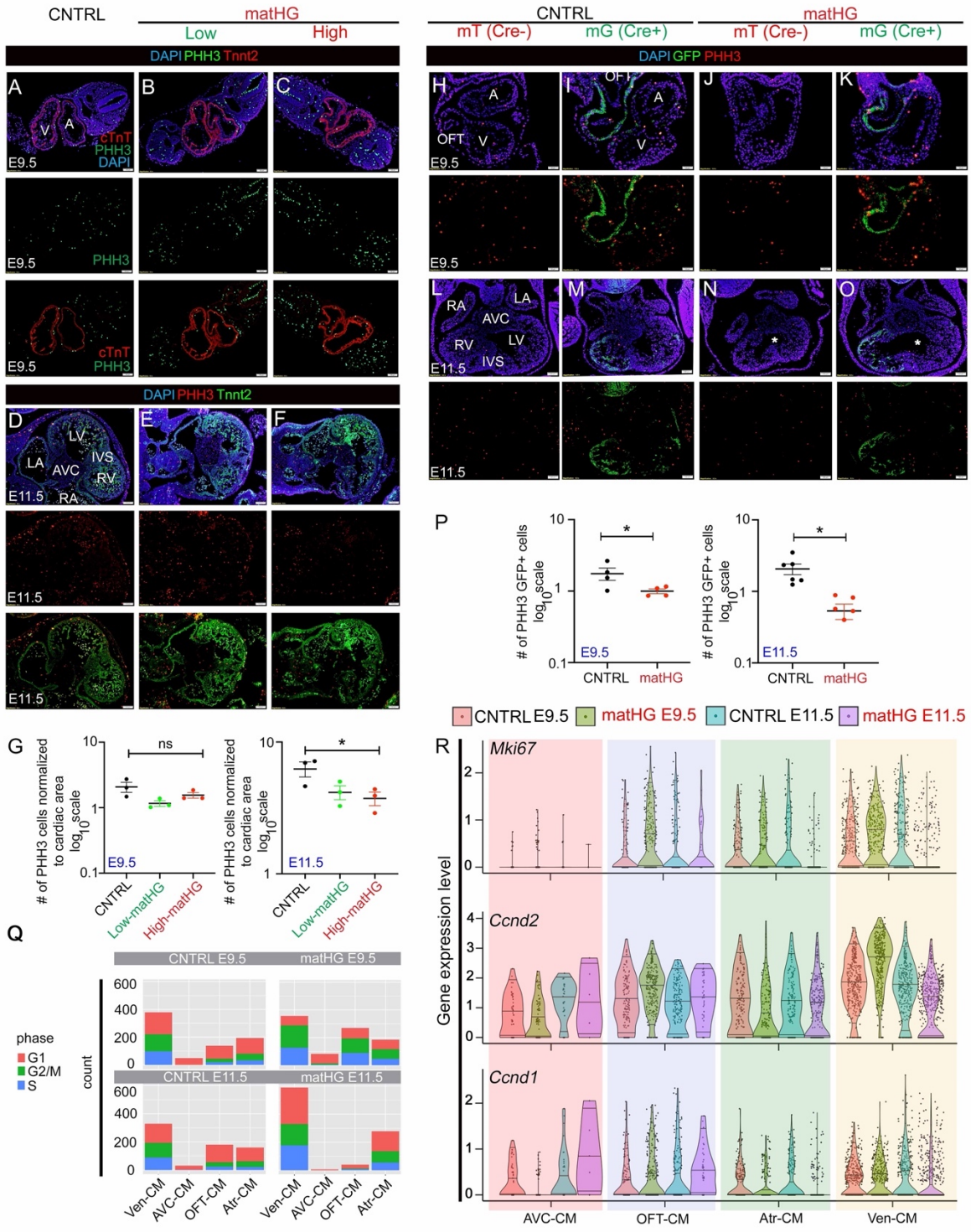
CNTRL
matHG
Low
High
DAPI PHH3 Tnnt2
A
B
C
V
A
cTnT
PHH3
DAPI
E9.5
PHH3
cTnT
PHH3
DAPI PHH3 Tnnt2
D
E
F
LV
LA
AVC
IVS
RV
RA
E11.5
CNTRL
matHG
mT (Cre-)
mG (Cre+)
mT (Cre-)
mG (Cre+)
DAPI GFP PHH3
H
I
J
K
OFT
A
V
E9.5
L
M
N
O
RA
LA
AVC
LV
RV
IVS
E11.5
P
# of PHH3 GFP+ cells
log10 scale
E9.5
E11.5
CNTRL
matHG
CNTRL E9.5
matHG E9.5
CNTRL E11.5
matHG E11.5
G
# of PHH3 cells normalized to cardiac area
log10 scale
ns
*
E9.5
E11.5
CNTRL
Low-matHG
High-matHG
Q
CNTRL E9.5
matHG E9.5
CNTRL E11.5
matHG E11.5
phase
G1
G2/M
S
count
Ven-CM
AVC-CM
OFT-CM
Atr-CM
R
Mki67
Ccnd2
Ccnd1
Gene expression level
AVC-CM
OFT-CM
Atr-CM
Ven-CM

Figure S7

Fig. S7. Maternal hyperglycemia reduces cardiomyocyte proliferation

(A-C) Immunofluorescent co-staining of PHH3 (green) and cTnT (red) show myocardial (CM) proliferation in control (CNTRL) vs. low and high levels of maternal hyperglycemia (matHG)-exposed E9.5 hearts and quantified in **(G)**. **(D-F)** Immunofluorescent co-staining of PHH3 (red) and cTnT (green) show CM proliferation in CNTRL vs. low and high-matHG-exposed E11.5 hearts and quantified in **(G)**. **(H-O)** Immunofluorescent co-staining of PHH3 (red) and GFP (green) show *Isl1*-derived CM proliferation in CNTRL vs. matHG-exposed E9.5 and E11.5 Cre- (mT) vs. Cre+ (mG) cardiac tissues. The $GFP^{+}PHH3^{+}$ cells are quantified in **(P)**. **(Q)** Cell count and regression analysis on myocardial subclusters using Seurat reveal count in cell-cycle phases (G1, S, and G2/M) in E9.5 and E11.5 embryonic hearts exposed to CNTRL vs. matHG. **(R)** Violin plots show normalized expression levels of cell proliferation markers *Mki67*, *Ccnd2,* and *Ccnd1* in myocardial subclusters obtained from CNTRL and matHG-exposed scRNA-seq data on wildtype E9.5 and E11.5 embryonic hearts. Scale bar: (A-F and L-N: 100µm and H-J: 50µm). Nuclei stained with DAPI in blue. A, atria; V, ventricle; LV, left ventricle; RV, right ventricle; AVC, atrioventricular canal; IVS, interventricular septum. OFT = outflow tract, Ven= ventricular, Atr= atrial, AVC-CM= atrioventricular cardiomyocytes. Data presented at mean $\pm$ SEM. ns= non-significant and * indicates two-tailed p-value<0.05.

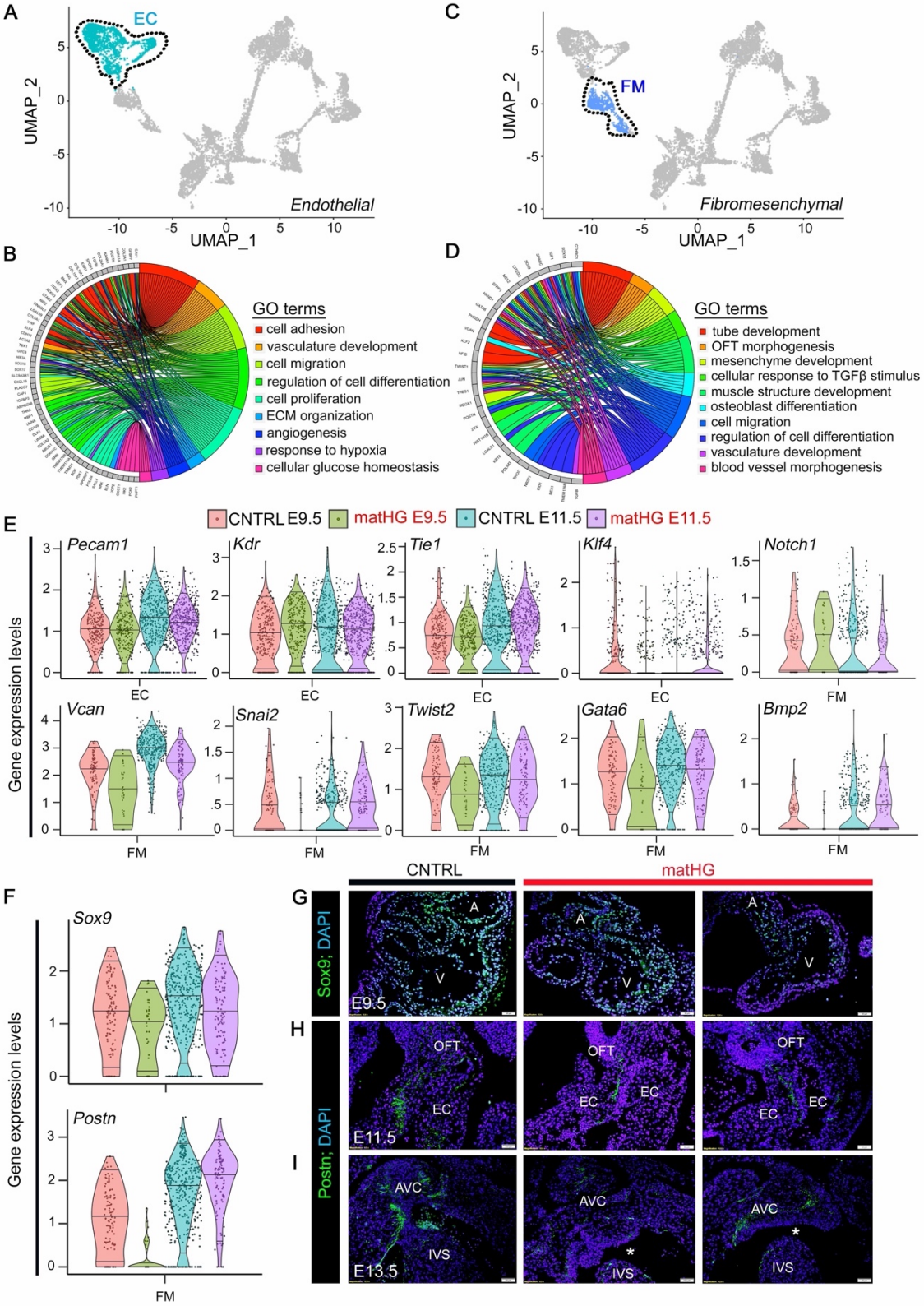
A
EC
UMAP_2
UMAP_1
Endothelial
C
FM
Fibromesenchymal
B
GO terms
cell adhesion
vasculature development
cell migration
regulation of cell differentiation
cell proliferation
ECM organization
angiogenesis
response to hypoxia
cellular glucose homeostasis
D
GO terms
tube development
OFT morphogenesis
mesenchyme development
cellular response to TGFβ stimulus
muscle structure development
osteoblast differentiation
cell migration
regulation of cell differentiation
vasculature development
blood vessel morphogenesis
E
CNTRL E9.5
matHG E9.5
CNTRL E11.5
matHG E11.5
Gene expression levels
Pecam1
Kdr
Tie1
Klf4
Notch1
Vcan
Snai2
Twist2
Gata6
Bmp2
EC
FM
F
Sox9
Postn
G
H
I
CNTRL
matHG
Sox9; DAPI
Postn; DAPI
E9.5
E11.5
E13.5
A
V
OFT
AVC
IVS

Figure S8

Fig. S8. Hyperglycemic exposure causes transcriptional changes in endocardial and mesenchymal cell populations

(A, B) The UMAP plots highlight the endothelial/endocardial (EC) and fibro-mesenchymal (FM) clusters from E9.5 and E11.5 embryonic hearts subjected to control (CNTRL) and maternal hyperglycemia (matHG) milieu. **(C, D)** Chord plots display differentially expressed genes in EC and FM clusters with their strongly associated Gene Ontology (GO) terms. **(E)** Violin plots show the normalized expression levels of genes in EC (*Pecam1, Kdr, Tie1, and Klf4*) and FM (*Vcan, Snai2, Twist2, Gata6, Bmp2, and Notch1*) clusters from CNTRL and matHG-exposed E9.5 and E11.5 embryonic hearts. **(F)** Marked reduction in *Sox9* and *Postn* gene-expression was noted in E9.5 and E11.5 FM populations. **(G-I)** Immunofluorescent staining corroborates the protein expression of Sox9 and Postn at E9.5, E11.5 and E13.5 hearts exposed to matHG vs. CNTRL dams. Scale bars: G-I; 50µm. Nuclei stained with DAPI in blue. A, atria; V, ventricle; OFT, outflow tract; EC, endocardial cushion; AVC, atrioventricular canal; IVS, interventricular septum.

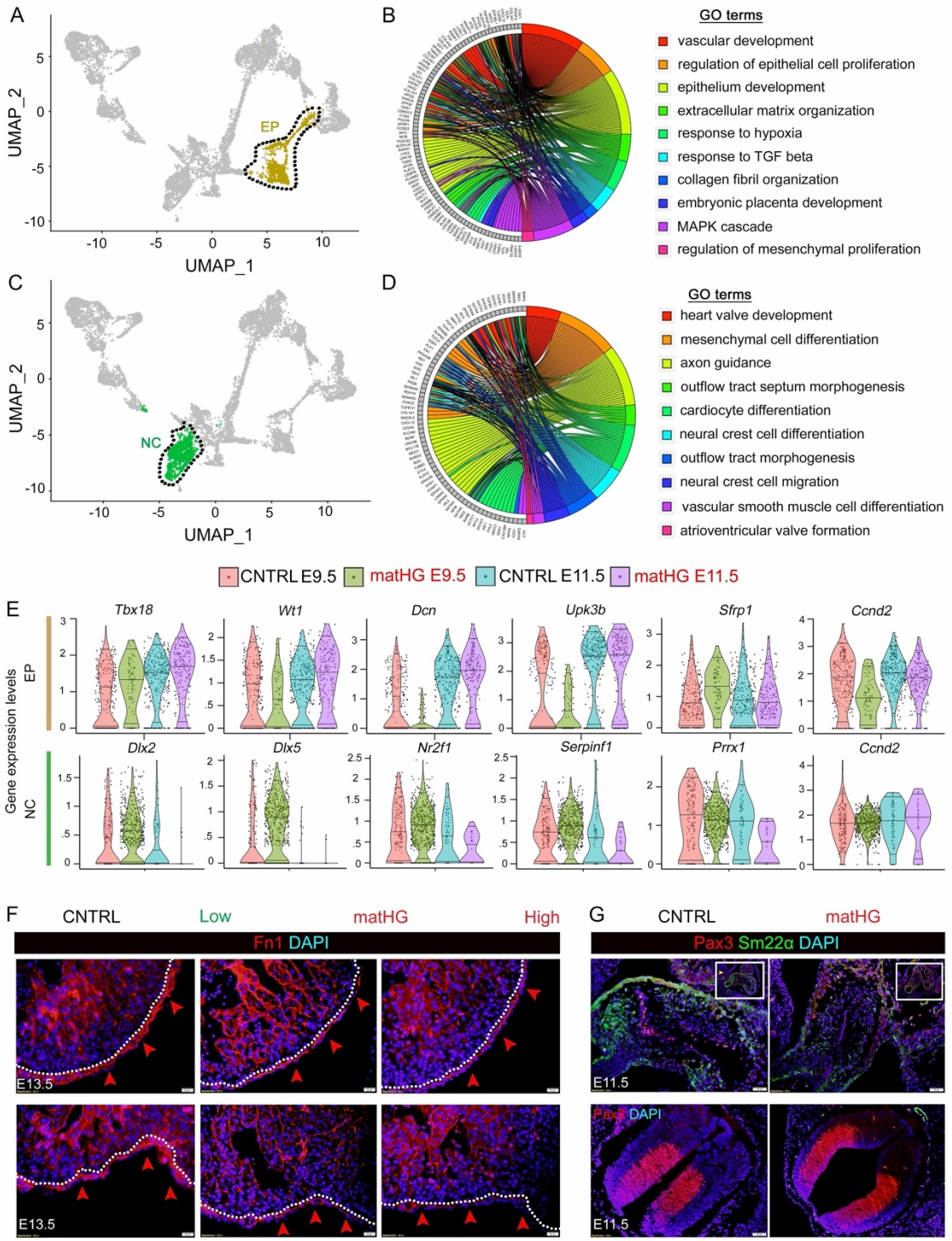
A
UMAP_2
UMAP_1
EP
B
GO terms
vascular development
regulation of epithelial cell proliferation
epithelium development
extracellular matrix organization
response to hypoxia
response to TGF beta
collagen fibril organization
embryonic placenta development
MAPK cascade
regulation of mesenchymal proliferation
C
UMAP_2
UMAP_1
NC
D
GO terms
heart valve development
mesenchymal cell differentiation
axon guidance
outflow tract septum morphogenesis
cardiocyte differentiation
neural crest cell differentiation
outflow tract morphogenesis
neural crest cell migration
vascular smooth muscle cell differentiation
atrioventricular valve formation
CNTRL E9.5
matHG E9.5
CNTRL E11.5
matHG E11.5
E
Gene expression levels
EP
NC
Tbx18
Wt1
Dcn
Upk3b
Sfrp1
Ccnd2
Dlx2
Dlx5
Nr2f1
Serpinf1
Prrx1
Ccnd2
F
CNTRL
Low
matHG
High
Fn1 DAPI
E13.5
E13.5
G
CNTRL
matHG
Pax3 Sm22α DAPI
E11.5
DAPI
E11.5

Figure S9

Fig. S9. Maternal hyperglycemia alters gene programs in epicardial and neural crest cells

(A, B) The UMAP plots highlight the epicardial (EP) and neural crest cell (NC) clusters from E9.5 and E11.5 embryonic hearts exposed to control (CNTRL) and maternal hyperglycemia (matHG). **(C, D)** Chord plots display differentially expressed genes in EP and NC clusters with their associated Gene Ontology (GO) terms. **(E)** Violin plots show the normalized expression levels of genes in EP (*Tbx18, Wt1, Dcn, Upk3b, Sfrp1, and Ccnd2*) and NC (*Dlx2, Dlx5, Nr2f1, Serpinf1, Prrx1, and Ccnd2*) clusters from CNTRL and matHG-exposed E9.5 and E11.5 embryonic hearts. **(F)** Immunofluorescent staining shows a gradual reduction in *Fn1* protein expression in the epicardium from low to high-matHG exposed E13.5 embryos compared to CNTRL, as indicated by the dotted white line. **(G)** Immunofluorescent co-staining of Pax3 (red) and Sm22α (green) demonstrate the reduction of Pax3 at E11.5 heart exposed to matHG vs. CNTRL, while no change in Pax3 expression was noted in the neural tube. Scale bars: F, 20µm and G, 50µm. DAPI stains the nuclei (blue).

Supplemental Tables:

Table S1. Distribution of *wildtype* embryos exposed to CNTRL, low and high-matHG environment

Maternal environment	Maternal B.G. ± stdev (# of litters)	Embryonic timepoint	# of embryos	2-tailed P-value (One-way ANOVA)
CNTRL	181.67 ± 18.3 (3)	E9.5	23	0.0032*
Low-matHG	243.00 ± 24.9 (3)		20	
High-matHG	327.7 ± 30.1 (3)		24	
			Total = 67	
CNTRL	195.3 ± 18.8 (3)	E11.5	25	0.0002*
Low-matHG	304.0 ± 14.7 (3)		23	
High-matHG	494.3 ± 46.3 (3)		23	
			Total = 71	
CNTRL	185.67 ± 23.47 (3)	E13.5	26	0.0148*
Low-matHG	265.67 ± 22.37 (3)		20	
High-matHG	519.33 ± 136.7 (3)		25	
			Total = 71	
CNTRL	193.7 ± 11.4 (3)	E15.5	21	0.0165*
Low-matHG	301.0 ± 9.9 (3)		26	
High-matHG	555.7 ± 152.9 (3)		24	
			Total = 71	

* indicates p-values to be statistically significant ($p<0.05$).

Table S2. List of DEGs in CNTRL vs. matHG-exposed E9.5 hearts.

Table S3. List of DEGs in CNTRL vs. matHG-exposed E11.5 hearts

Table S4. List of GO terms associated with DEGs in CNTRL vs. matHG-exposed E9.5 hearts

Table S5. List of GO terms associated with DEGs in CNTRL vs. matHG-exposed E11.5 hearts.

Table S6. List of DEGs in CNTRL vs. matHG exposed E9.5 MP-CM subclusters

Table S7. List of DEGs in CNTRL vs. matHG-exposed E11.5 MP-CM subclusters

Table S8. List of GO-terms in E9.5 and E11.5 MP-CM subclusters

Table S9. E9.5 DEG analysis of MP-CM monocle states

Table S10. E11.5 DEG analysis of MP-CM monocle states

Table S11: Distribution of *Isl1-Cre*$^{+/-}$; *Rosa*$^{mT/mG}$ embryos in the setting of NDM and high-matHG environment

Maternal Status	Maternal B.G ± SD (# of litters)	Embryonic timepoint	# of embryos	*Rosa*$^{mT/mG}$; *Cre-*	*Rosa*$^{mT/mG}$; *Cre+*	2-tailed P value (χ^2 test)
matNG	208.5 ± 7.5 (2)	E9.5	19	7	12	0.5542
matHG	335.0 ± 58.7 (3)		28	14	14	
matNG	205.3 ± 37.8 (3)	E11.5	22	14	8	0.2949
matHG	420.8 ±191.8 (4)		33	15	18	
matNG	244.7 ± 25.0 (3)	E13.5	26	13	13	0.9121
matHG	649.2 ± 78.1 (5)		35	17	18	